NFFT based Ewald summation for electrostatic systems with charges and dipoles

Michael Hofmann*

Chemnitz University of Technology, Faculty of Computer Science, 09107 Chemnitz, Germany

Franziska Nestler†, Michael Pippig‡

Chemnitz University of Technology, Faculty of Mathematics, 09107 Chemnitz, Germany

The efficient computation of Coulomb interactions in charged particle systems is of great importance in the field of molecular dynamics simulations. It is widely known that an approximation can be realized based on the Ewald summation approach and the fast Fourier transform (FFT). In the present paper we consider particle systems containing a mixture of N point charges as well as point dipoles. New cutoff errors in the Ewald summation formulas concerning charge-dipole interactions are derived and, moreover, validated by numerical examples. Furthermore, we present for the first time an $\mathcal{O}(N \log N)$ particle mesh algorithm for computing mixed charge-dipole interactions based on the FFT for nonequispaced data (NFFT). We present first numerical results for charge-dipole systems, showing that the introduced method can be tuned to a high precision and verifying the $\mathcal{O}(N \log N)$ scaling. In order to calculate the interactions with dipoles efficiently, two new variants of the NFFT, namely the Hessian NFFT as well as the adjoint gradient NFFT, are derived and implemented. In the context of NFFT, these new variants are of great importance on their own. The presented particle mesh method is an extension of the particle-particle NFFT (P^{2}NFFT) framework. Therefore, all the formerly derived P^{2}NFFT features, which cover for instance the treatment of arbitrary combinations of periodic and non-periodic boundary conditions, the handling of triclinic box shapes and a massively parallel implementation, are now also supported for mixed charge-dipole as well as pure dipole systems. The algorithms are publicly available as a part of the ScaFaCoS library.

Key words and phrases: Ewald summation, nonequispaced fast Fourier transform, particle methods, charged particle systems, dipole-dipole interactions, charge-dipole interactions, periodic boundary conditions, NFFT, P2NFFT, P3M, ScaFaCoS

2000 AMS Mathematics Subject Classification : 65T

1 Introduction

In this paper we consider electrostatic systems consisting of point charges as well as point dipoles and show how the interactions between these particles can be computed efficiently via the non-

*michael.hofmann@informatik.tu-chemnitz.de

†franziska.nestler@mathematik.tu-chemnitz.de

‡michael.pippig.tuc@gmail.com

equispaced FFT (NFFT). We present a particle mesh method capable of calculating electrostatic interactions in systems containing a mixture of charges and dipoles with an arithmetic complexity of $\mathcal{O}(N \log N)$, where N denotes the number of present particles. In the following we introduce the considered electrostatic quantities.

Given three linearly independent vectors $\boldsymbol{\ell}_1, \boldsymbol{\ell}_2, \boldsymbol{\ell}_3 \in \mathbb{R}^3$, the particles are assumed to be distributed in a box spanned by these three vectors. If periodic boundary conditions are applied in all three dimensions, the underlying space is the three-dimensional torus

$$\mathcal{T} := \boldsymbol{\ell}_1\mathbb{T} \times \boldsymbol{\ell}_2\mathbb{T} \times \boldsymbol{\ell}_3\mathbb{T} := \{\lambda_1\boldsymbol{\ell}_1 + \lambda_2\boldsymbol{\ell}_2 + \lambda_3\boldsymbol{\ell}_3 \mid \lambda_1, \lambda_2, \lambda_3 \in \mathbb{T}\},$$

where $\mathbb{T} := \mathbb{R}/\mathbb{Z} \simeq [-1/2, 1/2)$.

For N_c charges $q_j \in \mathbb{R}$ at positions $\boldsymbol{x}_j \in \mathcal{T}$, $j = 1, \dots, N_\mathrm{c}$, as well as N_d dipoles $\boldsymbol{\mu}_j \in \mathbb{R}^3$ at positions $\boldsymbol{x}_j \in \mathcal{T}$, $j = N_\mathrm{c}+1, \dots, N_\mathrm{c}+N_\mathrm{d}$, the overall electrostatic energy can be written as

$$U = \frac{1}{2}\sum_{j=1}^{N} \xi_j \phi(j) \tag{1.1}$$

with the potentials

$$\begin{aligned} \phi(j) &= {\sum_{\boldsymbol{n}\in\mathbb{Z}^3}}' \sum_{i=1}^{N} \frac{\xi_i}{\|\boldsymbol{x}_{ij} + \boldsymbol{L}\boldsymbol{n}\|} \\ &= {\sum_{\boldsymbol{n}\in\mathbb{Z}^3}}' \sum_{i=1}^{N_\mathrm{c}} \frac{q_i}{\|\boldsymbol{x}_{ij} + \boldsymbol{L}\boldsymbol{n}\|} - {\sum_{\boldsymbol{n}\in\mathbb{Z}^3}}' \sum_{i=N_\mathrm{c}+1}^{N} \frac{\boldsymbol{\mu}_i^\top(\boldsymbol{x}_{ij} + \boldsymbol{L}\boldsymbol{n})}{\|\boldsymbol{x}_{ij} + \boldsymbol{L}\boldsymbol{n}\|^3}. \end{aligned} \tag{1.2}$$

Thereby, we define the difference vectors $\boldsymbol{x}_{ij} := \boldsymbol{x}_i - \boldsymbol{x}_j$, the Euclidean norm is denoted by $\|\cdot\|$ and $N := N_\mathrm{c} + N_\mathrm{d}$ represents the total number of particles. Furthermore, the prime indicates that for $\boldsymbol{n} = \boldsymbol{0}$ all terms with $i = j$ are omitted and the regular matrix $\boldsymbol{L}$ is given by $\boldsymbol{L} := [\boldsymbol{\ell}_1, \boldsymbol{\ell}_2, \boldsymbol{\ell}_3]$. The operators ξ_j are defined via

$$\xi_j := \begin{cases} q_j & : j \in \{1, \dots, N_\mathrm{c}\}, \\ (\boldsymbol{\mu}_j^\top \nabla_{\boldsymbol{x}_j}) & : j \in \{N_\mathrm{c}+1, \dots, N\}. \end{cases}$$

The expressions for the energy (1.1) and the potentials (1.2) are the same as for charge-charge systems [14, 28], where the charges q_j have simply been replaced by the operators ξ_j. Note that the infinite sum in (1.2) is conditionally convergent, provided that we have charge neutrality, i.e.,

$$\sum_{j=1}^{N_\mathrm{c}} q_j = 0. \tag{1.3}$$

Thus, the value of the energy (1.1) strongly depends on the underlying summation order. Generally, a spherical order of summation is applied, see [28] for more details.

We are also interested in the computation of the fields $\boldsymbol{E}(j)$, energies $U(j)$ and forces $\boldsymbol{F}(j)$ of the single particles, which are given by

$$\boldsymbol{E}(j) := -\nabla_{\boldsymbol{x}_j}\phi(j) = {\sum_{\boldsymbol{n}\in\mathbb{Z}^3}}' \sum_{i=1}^{N_\mathrm{c}} \frac{q_i \boldsymbol{x}_{ij,\boldsymbol{n}}}{\|\boldsymbol{x}_{ij,\boldsymbol{n}}\|^3} + {\sum_{\boldsymbol{n}\in\mathbb{Z}^3}}' \sum_{i=N_\mathrm{c}+1}^{N} \left(\frac{3\boldsymbol{\mu}_i^\top \boldsymbol{x}_{ij,\boldsymbol{n}}}{\|\boldsymbol{x}_{ij,\boldsymbol{n}}\|^5} \boldsymbol{x}_{ij,\boldsymbol{n}} - \frac{\boldsymbol{\mu}_i}{\|\boldsymbol{x}_{ij,\boldsymbol{n}}\|^3} \right),$$

where we set $\boldsymbol{x}_{ij,\boldsymbol{n}} := \boldsymbol{x}_{ij} + \boldsymbol{L}\boldsymbol{n}$,

$$U(j) := \xi_j\phi(j) = \begin{cases} q_j\phi(j) & : j \in \{1, \dots, N_\mathrm{c}\}, \\ -\boldsymbol{\mu}_j^\top \boldsymbol{E}(j) & : j \in \{N_\mathrm{c}+1, \dots, N\}, \end{cases} \tag{1.4}$$

and

$$\boldsymbol{F}(j) := -\nabla_{\boldsymbol{x}_j} U(j) = \begin{cases} q_j \boldsymbol{E}(j) & : j \in \{1, \dots, N_\mathrm{c}\}, \\ \boldsymbol{G}(j)\boldsymbol{\mu}_j & : j \in \{N_\mathrm{c}+1, \dots, N\}, \end{cases} \tag{1.5}$$

where $\boldsymbol{G}(j) \in \mathbb{R}^{3\times 3}$ is the negative electric field gradient, i.e.,

$$\begin{aligned} \boldsymbol{G}(j) :=& -\nabla_{\boldsymbol{x}_j} \nabla_{\boldsymbol{x}_j}^\top \phi(j) \\ =& \sum_{\boldsymbol{n}\in\mathbb{Z}^3}{}' \sum_{i=1}^{N_\mathrm{c}} \left(\frac{q_i}{\|\boldsymbol{x}_{ij,\boldsymbol{n}}\|^3} \boldsymbol{I}_{3,3} - \frac{3q_i}{\|\boldsymbol{x}_{ij,\boldsymbol{n}}\|^5} \boldsymbol{x}_{ij,\boldsymbol{n}} \boldsymbol{x}_{ij,\boldsymbol{n}}^\top \right) \\ &+ \sum_{\boldsymbol{n}\in\mathbb{Z}^3}{}' \sum_{i=N_\mathrm{c}+1}^{N} \left(\frac{15\boldsymbol{\mu}_i^\top \boldsymbol{x}_{ij,\boldsymbol{n}}}{\|\boldsymbol{x}_{ij,\boldsymbol{n}}\|^7} \boldsymbol{x}_{ij,\boldsymbol{n}} \boldsymbol{x}_{ij,\boldsymbol{n}}^\top - \frac{3}{\|\boldsymbol{x}_{ij,\boldsymbol{n}}\|^5} (\boldsymbol{\mu}_i \boldsymbol{x}_{ij,\boldsymbol{n}}^\top + \boldsymbol{x}_{ij,\boldsymbol{n}} \boldsymbol{\mu}_i^\top) - \frac{3\boldsymbol{\mu}_i^\top \boldsymbol{x}_{ij,\boldsymbol{n}}}{\|\boldsymbol{x}_{ij,\boldsymbol{n}}\|^5} \boldsymbol{I}_{3,3} \right). \end{aligned}$$

We remark that the computation of sums of a very similar structure is required in order to solve Stokes equations in three dimensions, for which fast algorithms have been proposed recently, see [44, 26].

For the dipole particles, i.e., for $j = N_\mathrm{c}+1, \dots, N$, the torques are given by

$$\boldsymbol{\tau}(j) := \boldsymbol{\mu}_j \times \boldsymbol{E}(j). \tag{1.6}$$

Note that we can further simplify the expression of the overall energy (1.1) via

$$U = \frac{1}{2} \sum_{j=1}^{N_\mathrm{c}} q_j \phi(j) - \frac{1}{2} \sum_{j=N_\mathrm{c}+1}^{N} \boldsymbol{\mu}_j^\top \boldsymbol{E}(j), \tag{1.7}$$

i.e., the overall energy can be obtained easily after having computed the potentials of the charges as well as the fields of the dipoles.

There are already various algorithms for the computation of interactions in charged particle systems, such as the particle-particle particle-mesh ($\mathrm{P^3M}$) method [12, 19, 8], the particle-particle NFFT ($\mathrm{P^2NFFT}$) [18, 39], further so called particle mesh methods [7, 13], the fast multipole method [17] as well as multigrid-based methods [4], just to mention a few. Note that [2] includes a detailed comparison between different efficient methods for the 3d-periodic Coulomb problem. The results show that the $\mathrm{P^3M}$ and $\mathrm{P^2NFFT}$ solvers rank among the best methods in this field. Furthermore, for lattice structured systems an approach based on tensor approximation techniques has been proposed recently, see [25].

For systems containing point dipoles the $\mathrm{P^3M}$ for dipolar systems has already been introduced and applied successfully, see [6, 5]. In this paper we show how the introduced quantities can be approximated efficiently for systems containing charges as well as dipoles. Therefor, the $\mathrm{P^2NFFT}$ method [39, 33, 34] is extended appropriately. Consequently, we present for the first time an $\mathcal{O}(N \log N)$ algorithm for computing electrostatic interactions in charge-dipole systems. We remark that the modular structure enables the combination of the extended modules with all former developments, which covers for instance the usage on massively parallel architectures and the application of various types of periodic boundary conditions, i.e.,

$$\phi(j) := \sum_{\boldsymbol{n}\in\mathcal{S}}{}' \sum_{i=1}^{N} \frac{\xi_i}{\|\boldsymbol{x}_{ij} + \boldsymbol{L}\boldsymbol{n}\|}$$

with $\mathcal{S} = \mathbb{Z}^p \times \{0\}^{3-p}$ and the number $p \in \{0, 1, 2, 3\}$ of dimensions subject to periodic boundary conditions. In the present paper we concentrate on 3d-periodic boundary conditions, i.e., $p = 3$, as introduced above. Note that the generalization of the method for the computation of dipole-dipole interactions has already been presented in [31]. We emphasize that the issue of implementing as well as testing the described approach was left open in [31]. In the present work we present

for the first time details on the recently developed implementation as well as numerical results. We introduce our extension of the method, which enables the treatment of mixed charge-dipole systems, including pure charge and pure dipole systems as special cases.

Our method is based on the Ewald summation approach [14, 28], which we introduce in Section 2. In Section 3 we discuss the arising root mean square (rms) errors in the forces, which are introduced by truncating the Ewald sums. We revisit the known error estimates for charge-charge [27] as well as for dipole-dipole [46] systems and derive new estimates concerning the interactions between charges and dipoles. The NFFT is briefly described in Section 4. In the charge-charge case we need the NFFT as well as the adjoint NFFT in order to approximate the potentials of the charges and in addition the so called gradient NFFT for the approximation of the acting forces, see [39, 40, 38]. For systems containing both charges and dipoles we need new NFFT modules, which we call Hessian NFFT and adjoint gradient NFFT. These new NFFT modules are described in Section 4, as well. The final algorithm, which is publicly available as a part of the ScaFaCoS library [1], is summarized in Section 5, while its implementation is described in Section 6. In Section 7 we present new numerical results, verifying the correctness of the presented error estimates and showing that the method can be tuned to a high precision. Furthermore, we demonstrate the $\mathcal{O}(N \log N)$ scaling with the help of a proper numerical test. A summary is given in Section 8.

2 Ewald summation

Numerous methods in the field of particle simulation are based on the so called Ewald summation technique [14]. Thereby, the Ewald splitting

$$\frac{1}{r} = \frac{\operatorname{erfc}(\alpha r)}{r} + \frac{\operatorname{erf}(\alpha r)}{r}$$

is used, where $\alpha > 0$ is called Ewald or splitting parameter, $\operatorname{erf}(x) = 2\pi^{-1/2} \int_0^x \mathrm{e}^{-t^2} \mathrm{d}t$ is the well known error function and $\operatorname{erfc}(x) = 1 - \operatorname{erf}(x)$ is the complementary error function.

If the splitting is applied to (1.1) by setting $r := \|\boldsymbol{x}_{ij} + \boldsymbol{L}\boldsymbol{n}\|$ in each summand, the energy U is split into an absolutely converging short range part

$$U^{\mathrm{short}} = \frac{1}{2} \sum_{j=1}^{N} \xi_j \phi^{\mathrm{short}}(j) \quad \text{with} \quad \phi^{\mathrm{short}}(j) := \sum_{\boldsymbol{n} \in \mathbb{Z}^3}{}' \sum_{i=1}^{N} \xi_i \frac{\operatorname{erfc}(\alpha \|\boldsymbol{x}_{ij} + \boldsymbol{L}\boldsymbol{n}\|)}{\|\boldsymbol{x}_{ij} + \boldsymbol{L}\boldsymbol{n}\|} \tag{2.1}$$

as well as a long range part U^{long} including all erf terms.

A transform of the long range part into Fourier space yields $U^{\mathrm{long}} = U^{\mathrm{F}} - U^{\mathrm{self}} + U^{\mathbf{0}}$ with the following three sums. First, the Fourier sum is given by

$$U^{\mathrm{F}} = \frac{1}{2} \sum_{j=1}^{N} \xi_j \phi^{\mathrm{F}}(j) \quad \text{with} \quad \phi^{\mathrm{F}}(j) := \frac{1}{\pi V} \sum_{\boldsymbol{k} \in \mathbb{Z}^3} \hat{\psi}(\boldsymbol{k}) \left(\sum_{i=1}^{N} \xi_i \, \mathrm{e}^{2\pi \mathrm{i} \boldsymbol{k}^\top \boldsymbol{L}^{-1} \boldsymbol{x}_i} \right) \mathrm{e}^{-2\pi \mathrm{i} \boldsymbol{k}^\top \boldsymbol{L}^{-1} \boldsymbol{x}_j}, \tag{2.2}$$

where $V := |\det(\boldsymbol{L})|$ denotes the volume of the simulation box and the Fourier coefficients $\hat{\psi}(\boldsymbol{k})$ are given by

$$\hat{\psi}(\boldsymbol{k}) := \begin{cases} \dfrac{\mathrm{e}^{-\pi^2 \|\boldsymbol{L}^{-\top} \boldsymbol{k}\|^2 / \alpha^2}}{\|\boldsymbol{L}^{-\top} \boldsymbol{k}\|^2} & : \boldsymbol{k} \neq \boldsymbol{0}, \\ 0 & : \boldsymbol{k} = \boldsymbol{0}. \end{cases} \tag{2.3}$$

Second, the self energy

$$U^{\mathrm{self}} := \frac{\alpha}{\sqrt{\pi}} \sum_{j=1}^{N_{\mathrm{c}}} q_j^2 + \frac{2\alpha^3}{3\sqrt{\pi}} \sum_{j=N_{\mathrm{c}}+1}^{N} \|\boldsymbol{\mu}_j\|^2 =: \frac{1}{2} \sum_{j=1}^{N_{\mathrm{c}}} q_j \phi^{\mathrm{self}}(j) - \frac{1}{2} \sum_{j=N_{\mathrm{c}}+1}^{N} \boldsymbol{\mu}_j^\top \boldsymbol{E}^{\mathrm{self}}(j) \tag{2.4}$$

is subtracted in order to correct for the included terms with $\|\boldsymbol{x}_{ij} + \boldsymbol{L}\boldsymbol{n}\| = 0$. Finally, the correction term $U^{\mathbf{0}}$ is defined as

$$U^{\mathbf{0}} = \frac{1}{2}\sum_{j=1}^{N} \xi_j \phi^{\mathbf{0}}(j) \quad \text{with} \quad \phi^{\mathbf{0}}(j) := -\frac{2\pi}{3V}\sum_{i=1}^{N} \xi_i \|\boldsymbol{x}_{ij}\|^2. \tag{2.5}$$

In summary we have

$$U = U^{\text{short}} + U^{\text{F}} - U^{\text{self}} + U^{\mathbf{0}}.$$

For a detailed derivation we refer to [14, 28].

Remark 2.1. The correction term is the only term representing the order of summation as well as the type of the surrounding medium. In general, the prefactor of the correction energy is

$$-\frac{2\pi}{3V(1+\epsilon)},$$

where ϵ is the dielectric constant of the surrounding medium. For $\epsilon = 0$ we apply vacuum boundary conditions and end up with (2.5), whereas $\epsilon = +\infty$ corresponds to metallic boundary conditions.

For systems containing only charges the term $U^{\mathbf{0}}$ is generally known as the dipole correction term and is more precisely given by

$$U^{\mathbf{0}} = -\frac{\pi}{3V}\sum_{i,j=1}^{N_{\text{c}}} q_i q_j \|\boldsymbol{x}_{ij}\|^2 = \frac{2\pi}{3V}\left\|\sum_{i=1}^{N_{\text{c}}} q_i \boldsymbol{x}_i\right\|^2,$$

where the second identity follows from the charge neutrality condition (1.3). The correction term for mixed systems (2.5) is obtained by replacing the charges q_i by the operators ξ_i. Expressed in terms of the potentials we obtain

$$\phi^{\mathbf{0}}(j) = -\frac{2\pi}{3V}\sum_{i=1}^{N} \xi_i \|\boldsymbol{x}_{ij}\|^2 = \frac{4\pi}{3V}\left(\boldsymbol{D}_{\text{c}}^{\top}\boldsymbol{x}_j - \frac{1}{2}\sum_{i=1}^{N_{\text{c}}} q_i \|\boldsymbol{x}_i\|^2 - \sum_{i=N_{\text{c}}+1}^{N} \boldsymbol{\mu}_i^{\top}\boldsymbol{x}_i + \boldsymbol{D}_{\text{d}}^{\top}\boldsymbol{x}_j\right),$$

where we define the overall dipole moments

$$\boldsymbol{D}_{\text{c}} := \sum_{i=1}^{N_{\text{c}}} q_i \boldsymbol{x}_i \quad \text{and} \quad \boldsymbol{D}_{\text{d}} := \sum_{i=N_{\text{c}}+1}^{N} \boldsymbol{\mu}_i.$$

For the fields we obtain

$$\boldsymbol{E}^{\mathbf{0}}(j) = -\nabla_{\boldsymbol{x}_j}\phi^{\mathbf{0}}(j) = -\frac{4\pi}{3V}\left(\boldsymbol{D}_{\text{c}} + \boldsymbol{D}_{\text{d}}\right).$$

In summary we obtain for the correction energy

$$U^{\mathbf{0}} = \frac{1}{2}\sum_{j=1}^{N_{\text{c}}} q_j \phi^{\mathbf{0}}(j) - \frac{1}{2}\sum_{j=N_{\text{c}}+1}^{N} \boldsymbol{\mu}_j^{\top}\boldsymbol{E}^{\mathbf{0}}(j) = \frac{2\pi}{3V}\left(\|\boldsymbol{D}_{\text{c}}\|^2 + 2\boldsymbol{D}_{\text{c}}^{\top}\boldsymbol{D}_{\text{d}} + \|\boldsymbol{D}_{\text{d}}\|^2\right).$$

□

3 Cutoff errors in the Ewald formulas – an extension to charge-dipole systems

In the field of molecular dynamics simulations the root mean square (rms) error in the forces is commonly considered in order to measure the accuracy of an algorithm. We denote the rms force errors for the charges and for the dipoles by

$$\Delta F_{\text{c}} := \sqrt{\frac{1}{N_{\text{c}}}\sum_{j=1}^{N_{\text{c}}} \|\boldsymbol{F}(j) - \boldsymbol{F}_{\approx}(j)\|^2} \tag{3.1}$$

and

$$\Delta F_{\mathrm{d}} := \sqrt{\frac{1}{N_{\mathrm{d}}} \sum_{j=N_{\mathrm{c}}+1}^{N} \|\boldsymbol{F}(j) - \boldsymbol{F}_{\approx}(j)\|^2}, \tag{3.2}$$

respectively, where $\boldsymbol{F}_{\approx}(j)$ denote approximations of the exact forces $\boldsymbol{F}(j)$.

Both, the short range part as well as the Fourier space part, are converging exponentially fast and can thus be truncated. In the following we show how the arising rms errors in the forces caused by the truncation of the Ewald sums can be estimated. Thereby, we revisit the estimates for charge-charge as well as dipole-dipole interactions, as already considered in the literature, and present new estimates concerning interactions between charges and dipoles.

The NFFT based approximation of the truncated Fourier space part, as described above, introduce further approximation errors, which are not discussed here.

3.1 Rms force error in the short range part

In the following we denote the kernel function of the short range part shortly by

$$f(r) := \frac{\operatorname{erfc}(\alpha r)}{r}. \tag{3.3}$$

Furthermore, we set

$$\boldsymbol{x}_{ij,\boldsymbol{n}} := \boldsymbol{x}_{ij} + \boldsymbol{L}\boldsymbol{n} \quad \text{and} \quad r_{ij,\boldsymbol{n}} := \|\boldsymbol{x}_{ij,\boldsymbol{n}}\|.$$

Rms force errors for the charges

For the charges, i.e., for all $j = 1, \ldots, N_{\mathrm{c}}$, the short range part of the force $\boldsymbol{F}(j) = -q_j \nabla_{\boldsymbol{x}_j} \phi(j)$ can be written as

$$\boldsymbol{F}^{\mathrm{short}}(j) = \boldsymbol{F}^{\mathrm{short}}_{\mathrm{c.c.}}(j) + \boldsymbol{F}^{\mathrm{short}}_{\mathrm{c.d.}}(j),$$

where the first term

$$\boldsymbol{F}^{\mathrm{short}}_{\mathrm{c.c.}}(j) = -q_j \nabla_{\boldsymbol{x}_j} \sum_{i=1}^{N_{\mathrm{c}}} {\sum_{\boldsymbol{n}\in\mathbb{Z}^3}}' q_i f(r_{ij,\boldsymbol{n}}) = q_j \sum_{i=1}^{N_{\mathrm{c}}} {\sum_{\boldsymbol{n}\in\mathbb{Z}^3}}' q_i f'(r_{ij,\boldsymbol{n}}) \frac{\boldsymbol{x}_{ij,\boldsymbol{n}}}{r_{ij,\boldsymbol{n}}},$$

includes all charge-charge (c.c.) interactions, while the second term

$$\begin{aligned} \boldsymbol{F}^{\mathrm{short}}_{\mathrm{c.d.}}(j) &= -q_j \nabla_{\boldsymbol{x}_j} \sum_{i=N_{\mathrm{c}}+1}^{N} \sum_{\boldsymbol{n}\in\mathbb{Z}^3} \boldsymbol{\mu}_i^{\top} \nabla_{\boldsymbol{x}_i} f(r_{ij,\boldsymbol{n}}) \\ &= q_j \sum_{i=N_{\mathrm{c}}+1}^{N} \sum_{\boldsymbol{n}\in\mathbb{Z}^3} f''(r_{ij,\boldsymbol{n}}) \boldsymbol{\mu}_i^{\top} \boldsymbol{x}_{ij,\boldsymbol{n}} \frac{\boldsymbol{x}_{ij,\boldsymbol{n}}}{r_{ij,\boldsymbol{n}}^2} + f'(r_{ij,\boldsymbol{n}}) \left(\frac{\boldsymbol{\mu}_i}{r_{ij,\boldsymbol{n}}} - \boldsymbol{\mu}_i^{\top} \boldsymbol{x}_{ij,\boldsymbol{n}} \frac{\boldsymbol{x}_{ij,\boldsymbol{n}}}{r_{ij,\boldsymbol{n}}^3} \right) \end{aligned} \tag{3.4}$$

includes all contributions originating from charge-dipole (c.d.) interactions.

From now we denote by $r_{\mathrm{cut}} > 0$ the near field cutoff radius and approximate the short range part via considering only distances $r_{ij,\boldsymbol{n}}$ smaller than r_{cut}. The resulting approximation error, measured in the Euclidean norm, is denoted by

$$\delta F^{\mathrm{short}}_{\mathrm{c.c.}}(j) := \left\| q_j \sum_{i=1}^{N_{\mathrm{c}}} q_i {\sum_{\substack{\boldsymbol{n}\in\mathbb{Z}^3 \\ r_{ij,\boldsymbol{n}} > r_{\mathrm{cut}}}}}' f'(r_{ij,\boldsymbol{n}}) \frac{\boldsymbol{x}_{ij,\boldsymbol{n}}}{r_{ij,\boldsymbol{n}}} \right\|.$$

In the following we present an estimate of the corresponding rms error

$$\Delta F^{\mathrm{short}}_{\mathrm{c.c.}} := \sqrt{\frac{1}{N_{\mathrm{c}}} \sum_{j=1}^{N_{\mathrm{c}}} \delta F^{\mathrm{short}}_{\mathrm{c.c.}}(j)^2},$$

which has already been considered in [27], before extending the theory to charge-dipole interactions. Thereby, we will denote by

$$Q := \sum_{i=1}^{N_\mathrm{c}} q_i^2$$

the sum over all squared charge values.

The error is estimated as presented in [27] via

$$\delta F_\mathrm{c.c.}^\mathrm{short}(j)^2 \approx \frac{q_j^2 Q}{V} \int_0^{2\pi} \mathrm{d}\phi \int_0^{\pi} \sin\theta \mathrm{d}\theta \int_{r_\mathrm{cut}}^{\infty} \left\| f'(r) \frac{\boldsymbol{r}}{r} \right\|^2 r^2 \mathrm{d}r,$$

where

$$f'(r) = -\frac{2\alpha}{\sqrt{\pi} r} \mathrm{e}^{-\alpha^2 r^2} - \frac{\mathrm{erfc}(\alpha r)}{r^2}.$$

Thus, we obtain

$$\begin{aligned}
\delta F_\mathrm{c.c.}^\mathrm{short}(j)^2 &\approx \frac{4\pi q_j^2 Q}{V} \int_{r_\mathrm{cut}}^{\infty} \left(\frac{2\alpha}{\sqrt{\pi} r} \mathrm{e}^{-\alpha^2 r^2} + \frac{\mathrm{erfc}(\alpha r)}{r^2} \right)^2 r^2 \mathrm{d}r \\
&\approx \frac{q_j^2 Q r_\mathrm{cut}}{V \alpha^2} \mathrm{e}^{-2\alpha^2 r_\mathrm{cut}^2} \left(\frac{2\alpha}{\sqrt{\pi} r_\mathrm{cut}} + \frac{1}{\sqrt{\pi} \alpha r_\mathrm{cut}^3} \right)^2,
\end{aligned}$$

see [27]. Thereby, the asymptotic expansion formula

$$\int_A^{\infty} \mathrm{e}^{-Bx^2} f(x) \mathrm{d}x \approx \mathrm{e}^{-BA^2} \frac{f(A)}{2AB} \quad \text{if} \quad \frac{\mathrm{d}}{\mathrm{d}x} \frac{f(x)}{2Bx} \ll f(x) \; \forall\, x \geq A, \tag{3.5}$$

is applied two times. In case of the complementary error function we obtain

$$\mathrm{erfc}(x) = \frac{2}{\sqrt{\pi}} \int_x^{\infty} \mathrm{e}^{-x^2} \mathrm{d}x \approx \frac{\mathrm{e}^{-x^2}}{\sqrt{\pi} x}, \tag{3.6}$$

which is used first, followed by approximating the outer integral. Of course, this is only allowed provided that r_cut is chosen not too small.

The corresponding rms error can thus be approximated by

$$\Delta F_\mathrm{c.c.}^\mathrm{short} := \sqrt{\frac{1}{N_\mathrm{c}} \sum_{j=1}^{N_\mathrm{c}} \delta F_\mathrm{c.c.}^\mathrm{short}(j)^2} \approx \frac{Q\sqrt{r_\mathrm{cut}}}{\sqrt{N_\mathrm{c} V \alpha}} \mathrm{e}^{-\alpha^2 r_\mathrm{cut}^2} \left(\frac{2\alpha}{\sqrt{\pi} r_\mathrm{cut}} + \frac{1}{\sqrt{\pi} \alpha r_\mathrm{cut}^3} \right). \tag{3.7}$$

In the following we derive a corresponding estimate concerning the charge-dipole interaction, which is done in an analog manner. Thereby we denote by $\theta := \sphericalangle(\boldsymbol{\mu}_i, \boldsymbol{r})$ the angle between the dipole moment $\boldsymbol{\mu}_i$ and the vector $\boldsymbol{r}$. We obtain for the single contributions to the error, cf. (3.4),

$$\begin{aligned}
&\left\| f''(r) \boldsymbol{\mu}_i^\top \boldsymbol{r} \frac{\boldsymbol{r}}{r^2} + f'(r) \left(\frac{\boldsymbol{\mu}_i}{r} - \boldsymbol{\mu}_i^\top \boldsymbol{r} \frac{\boldsymbol{r}}{r^3} \right) \right\|^2 \\
&= \left\| f''(r) \|\boldsymbol{\mu}_i\| \cos(\theta) \frac{\boldsymbol{r}}{r} + f'(r) \left(\frac{\boldsymbol{\mu}_i}{r} - \|\boldsymbol{\mu}_i\| \cos(\theta) \frac{\boldsymbol{r}}{r^2} \right) \right\|^2 \\
&= \left(\tfrac{f''(r)}{r} - \tfrac{f'(r)}{r^2} \right)^2 r^2 \|\boldsymbol{\mu}_i\|^2 \cos^2\theta + \tfrac{f'(r)^2}{r^2} \|\boldsymbol{\mu}_i\|^2 + 2 \left(\tfrac{f''(r)}{r} - \tfrac{f'(r)}{r^2} \right) \tfrac{f'(r)}{r} \cos(\theta) \|\boldsymbol{\mu}_i\| \boldsymbol{\mu}_i^\top \boldsymbol{r} \\
&= \|\boldsymbol{\mu}_i\|^2 \left(\tfrac{f'(r)^2}{r^2} + \cos^2\theta \left(f''(r)^2 - \tfrac{f'(r)^2}{r^2} \right) \right).
\end{aligned}$$

Thus, we can approximate the error measured in the $\mathcal{L}_2$-norm by

$$\begin{aligned}\delta F_{\text{c.d.}}^{\text{short}}(j)^2 &\approx \frac{q_j^2}{V}\sum_{i=N_\text{c}+1}^{N}\int_0^{2\pi}\int_0^{\pi}\sin\theta\int_{r_\text{cut}}^{\infty} r^2\left\|f''(r)\boldsymbol{\mu}_i^\top\boldsymbol{r}\frac{\boldsymbol{r}}{r^2}+f(r)'\left(\frac{\boldsymbol{\mu}_i}{r}-\boldsymbol{\mu}_i^\top\boldsymbol{r}\frac{\boldsymbol{r}}{r^3}\right)\right\|^2\mathrm{d}r\mathrm{d}\theta\mathrm{d}\phi\\ &= \frac{2\pi q_j^2}{V}\sum_{i=N_\text{c}+1}^{N}\|\boldsymbol{\mu}_i\|^2\int_0^{\pi}\sin\theta\int_{r_\text{cut}}^{\infty} f'(r)^2+\cos^2\theta\left(r^2f''(r)^2-f'(r)^2\right)\mathrm{d}r\mathrm{d}\theta\\ &= \frac{2\pi q_j^2}{V}\sum_{i=N_\text{c}+1}^{N}\|\boldsymbol{\mu}_i\|^2\int_{r_\text{cut}}^{\infty}\tfrac{4}{3}f'(r)^2+\tfrac{2}{3}r^2f''(r)^2\mathrm{d}r,\end{aligned}\tag{3.8}$$

analogously to the approximation of $\delta F_{\text{c.c.}}^{\text{short}}(j)$.

The second derivative f'' of the function, as given in (3.3), can be written in the form

$$f''(r)=\frac{4\alpha^3}{\sqrt{\pi}}\mathrm{e}^{-\alpha^2r^2}+\frac{4\alpha}{\sqrt{\pi}r^2}\mathrm{e}^{-\alpha^2r^2}+2\frac{\operatorname{erfc}(\alpha r)}{r^3}\approx\frac{\mathrm{e}^{-\alpha^2r^2}}{\sqrt{\pi}\alpha r^4}\left(4\alpha^4r^4+4\alpha^2r^2+2\right).$$

Thereby, the approximation is again obtained via applying the asymptotic expansion formula (3.6) of the complementary error function.

By inserting the obtained approximations for the derivatives of f into (3.8) and making use of the asymptotic expansion (3.5) we obtain

$$\delta F_{\text{c.d.}}^{\text{short}}(j)^2\approx\frac{4\pi q_j^2\mathcal{M}}{3V}\cdot\frac{\mathrm{e}^{-2\alpha^2r_\text{cut}^2}}{4r_\text{cut}\alpha^2}\cdot\frac{1}{\pi\alpha^2r_\text{cut}^6}\left(2B_\text{cut}^2+(4\alpha^4r_\text{cut}^4+2B_\text{cut})^2\right)$$

with

$$B_\text{cut}:=1+2\alpha^2r_\text{cut}^2$$

and

$$\mathcal{M}:=\sum_{i=N_\text{c}+1}^{N}\|\boldsymbol{\mu}_i\|^2.$$

The corresponding rms error can be approximated by

$$\Delta F_{\text{c.d.}}^{\text{short}}:=\sqrt{\frac{1}{N_\text{c}}\sum_{j=1}^{N_\text{c}}\delta F_{\text{c.d.}}^{\text{short}}(j)^2}\approx\frac{\mathrm{e}^{-\alpha^2r_\text{cut}^2}}{\alpha^2r_\text{cut}^3}\sqrt{\frac{2Q\mathcal{M}}{3N_\text{c}Vr_\text{cut}}(3B_\text{cut}^2+8\alpha^4r_\text{cut}^4B_\text{cut}+8\alpha^8r_\text{cut}^8)}.\tag{3.9}$$

Assuming that the contributions originating from interactions with charges and those resulting from interactions with dipoles are independent, we may approximate the rms near field error in the forces of the charges via

$$\Delta F_\text{c}^{\text{short}}\approx\sqrt{\left(\Delta F_{\text{c.c.}}^{\text{short}}\right)^2+\left(\Delta F_{\text{c.d.}}^{\text{short}}\right)^2}.\tag{3.10}$$

Rms force errors for the dipole particles

For the dipoles, i.e., for all $j=N_\text{c}+1,\ldots,N$, the short range parts of the forces $\boldsymbol{F}(j)=-\nabla_{\boldsymbol{x}_j}\boldsymbol{\mu}_j^\top\nabla_{\boldsymbol{x}_j}\phi(j)$ are given by

$$\boldsymbol{F}^{\text{short}}(j)=\boldsymbol{F}_{\text{d.c.}}^{\text{short}}(j)+\boldsymbol{F}_{\text{d.d.}}^{\text{short}}(j),$$

where

$$\begin{aligned}
\boldsymbol{F}^{\text{short}}_{\text{d.c.}}(j) &= -\nabla_{\boldsymbol{x}_j}\boldsymbol{\mu}_j^\top\nabla_{\boldsymbol{x}_j}\sum_{i=1}^{N_\text{c}}\sum_{\boldsymbol{n}\in\mathbb{Z}^3} q_i f(r_{ij,\boldsymbol{n}}) \\
&= -\sum_{i=1}^{N_\text{c}} q_i \sum_{\boldsymbol{n}\in\mathbb{Z}^3} f''(r_{ij,\boldsymbol{n}})\boldsymbol{\mu}_j^\top\boldsymbol{x}_{ij,\boldsymbol{n}}\frac{\boldsymbol{x}_{ij,\boldsymbol{n}}}{r_{ij,\boldsymbol{n}}^2} + f'(r_{ij,\boldsymbol{n}})\left(\frac{\boldsymbol{\mu}_j}{r_{ij,\boldsymbol{n}}} - \frac{\boldsymbol{\mu}_j^\top\boldsymbol{x}_{ij,\boldsymbol{n}}}{r_{ij,\boldsymbol{n}}^3}\boldsymbol{x}_{ij,\boldsymbol{n}}\right), \\
\boldsymbol{F}^{\text{short}}_{\text{d.d.}}(j) &= -\nabla_{\boldsymbol{x}_j}\boldsymbol{\mu}_j^\top\nabla_{\boldsymbol{x}_j}\sum_{i=N_\text{c}+1}^{N}{\sum_{\boldsymbol{n}\in\mathbb{Z}^3}}' \boldsymbol{\mu}_i^\top\nabla_{\boldsymbol{x}_i} f(r_{ij,\boldsymbol{n}}) \\
&= -\sum_{i=N_\text{c}+1}^{N}{\sum_{\boldsymbol{n}\in\mathbb{Z}^3}}' C(r_{ij,\boldsymbol{n}})\left((\boldsymbol{\mu}_i^\top\boldsymbol{x}_{ij,\boldsymbol{n}})\boldsymbol{\mu}_j + (\boldsymbol{\mu}_j^\top\boldsymbol{x}_{ij,\boldsymbol{n}})\boldsymbol{\mu}_i + (\boldsymbol{\mu}_i^\top\boldsymbol{\mu}_j)\boldsymbol{x}_{ij,\boldsymbol{n}}\right) \\
&\quad + \sum_{i=N_\text{c}+1}^{N}{\sum_{\boldsymbol{n}\in\mathbb{Z}^3}}' D(r_{ij,\boldsymbol{n}})(\boldsymbol{\mu}_i^\top\boldsymbol{x}_{ij,\boldsymbol{n}})(\boldsymbol{\mu}_j^\top\boldsymbol{x}_{ij,\boldsymbol{n}})\boldsymbol{x}_{ij,\boldsymbol{n}}.
\end{aligned}$$

The functions C and D are given by

$$\begin{aligned}
C(r) &:= \frac{f''(r)}{r^2} - \frac{f'(r)}{r^3} = \frac{4\alpha^3}{\sqrt{\pi}r^2}\mathrm{e}^{-\alpha^2r^2} + \frac{6\alpha}{\sqrt{\pi}r^4}\mathrm{e}^{-\alpha^2r^2} + \frac{3\operatorname{erfc}(\alpha r)}{r^5}, \\
D(r) &:= -\frac{f'''(r)}{r^3} + 3\frac{f''(r)}{r^4} - 3\frac{f'(r)}{r^2} = \left(\frac{8\alpha^5}{\sqrt{\pi}r^2} + \frac{20\alpha^3}{\sqrt{\pi}r^4} + \frac{30\alpha}{\sqrt{\pi}r^6}\right)\mathrm{e}^{-\alpha^2r^2} + \frac{15\operatorname{erfc}(\alpha r)}{r^7},
\end{aligned}$$

see [46].

The same steps, which led to the approximation of $\delta F^{\text{short}}_{\text{c.d.}}(j)$ and $\Delta F^{\text{short}}_{\text{c.d.}}$, give

$$\delta F^{\text{short}}_{\text{d.c.}}(j)^2 \approx \frac{\|\boldsymbol{\mu}_j\|^2 Q\,\mathrm{e}^{-2\alpha^2r_\text{cut}^2}}{3V\alpha^4 r_\text{cut}^7}\left(2B_\text{cut}^2 + (4\alpha^4r_\text{cut}^4 + 2B_\text{cut}^2)\right)$$

for all $j = N_\text{c}+1,\dots,N$ as well as

$$\Delta F^{\text{short}}_{\text{d.c.}} := \sqrt{\frac{1}{N_\text{d}}\sum_{j=N_\text{c}+1}^{N}\delta F^{\text{short}}_{\text{d.c.}}(j)^2} \approx \frac{\mathrm{e}^{-\alpha^2r_\text{cut}^2}}{\alpha^2r_\text{cut}^3}\sqrt{\frac{2Q\mathcal{M}}{3N_\text{d}Vr_\text{cut}}\left(3B_\text{cut}^2 + 8\alpha^4r_\text{cut}^4B_\text{cut} + 8\alpha^8r_\text{cut}^8\right)}. \tag{3.11}$$

In the case of dipole-dipole interactions we refer to the derivation of the corresponding rms errors as presented in [46]. The final result reads as

$$\begin{aligned}
\Delta F^{\text{short}}_{\text{d.d.}} &:= \sqrt{\frac{1}{N_\text{d}}\sum_{j=N_\text{c}+1}^{N}\delta F^{\text{short}}_{\text{d.d.}}(j)^2} \\
&\approx \frac{\mathrm{e}^{-\alpha^2r_\text{cut}^2}\mathcal{M}}{\alpha^2r_\text{cut}^4}\sqrt{\frac{1}{r_\text{cut}N_\text{d}V}\left(\frac{13}{6}C_\text{cut}^2 + \frac{2}{15}D_\text{cut}^2 + \frac{13}{15}C_\text{cut}D_\text{cut}\right)},
\end{aligned} \tag{3.12}$$

where

$$\begin{aligned}
C_\text{cut} &:= 4\alpha^4r_\text{cut}^4 + 6\alpha^2r_\text{cut}^2 + 3, \\
D_\text{cut} &:= 8\alpha^6r_\text{cut}^6 + 20\alpha^4r_\text{cut}^4 + 30\alpha^2r_\text{cut}^2 + 15.
\end{aligned}$$

Assuming that the contributions originating from interactions with charges and those resulting from interactions with the other dipoles are independent, we may approximate the rms near field error in the forces of the dipoles via

$$\Delta F^{\text{short}}_\text{d} \approx \sqrt{\left(\Delta F^{\text{short}}_{\text{d.c.}}\right)^2 + \left(\Delta F^{\text{short}}_{\text{d.d.}}\right)^2}. \tag{3.13}$$

3.2 Rms force error in the Fourier space part

For some $\boldsymbol{M} \in 2\mathbb{N}^3$ we define the index set $\mathcal{I}_{\boldsymbol{M}}$ by

$$\mathcal{I}_{\boldsymbol{M}} := \left\{-\tfrac{M_1}{2}, \dots, \tfrac{M_1}{2} - 1\right\} \times \dots \times \left\{-\tfrac{M_3}{2}, \dots, \tfrac{M_3}{2} - 1\right\}.$$

Since the Fourier coefficients (2.3) decrease exponentially fast for growing $\boldsymbol{k}$ we can replace the infinite lattice by a finite lattice

$$\mathbb{Z}^3 \mapsto \mathcal{I}_{\boldsymbol{M}},$$

where $\boldsymbol{M} \in 2\mathbb{N}^3$ has to be chosen appropriately.

In the following we denote by

$$\tilde{\boldsymbol{\ell}}_1, \tilde{\boldsymbol{\ell}}_2, \tilde{\boldsymbol{\ell}}_3$$

the dual lattice vectors fulfilling $\tilde{\boldsymbol{\ell}}_i \cdot \boldsymbol{\ell}_j = \delta_{ij}$. The dual lattice vectors are simply the columns of the matrix $\boldsymbol{L}^{-\top}$.

We obtain

$$\|\boldsymbol{L}^{-\top}\boldsymbol{k}\|^2 = \|k_1\tilde{\boldsymbol{\ell}}_1 + k_2\tilde{\boldsymbol{\ell}}_2 + k_3\tilde{\boldsymbol{\ell}}_3\|^2.$$

Furthermore, we set

$$\boldsymbol{n}_{kl} := \tilde{\boldsymbol{\ell}}_k \times \tilde{\boldsymbol{\ell}}_l$$

and choose the cutoff parameters $c_1, c_2, c_3 \in \mathbb{R}_+$ such that

$$c_1\|\tilde{\boldsymbol{\ell}}_1\| \cdot |\cos \sphericalangle(\tilde{\boldsymbol{\ell}}_1, \boldsymbol{n}_{23})| = c_2\|\tilde{\boldsymbol{\ell}}_2\| \cdot |\cos \sphericalangle(\tilde{\boldsymbol{\ell}}_2, \boldsymbol{n}_{13})| = c_3\|\tilde{\boldsymbol{\ell}}_3\| \cdot |\cos \sphericalangle(\tilde{\boldsymbol{\ell}}_3, \boldsymbol{n}_{12})| = \beta, \tag{3.14}$$

where $\beta > 0$. This means that the three heights of the parallelepiped

$$\{x_1\tilde{\boldsymbol{\ell}}_1 + x_2\tilde{\boldsymbol{\ell}}_2 + x_3\tilde{\boldsymbol{\ell}}_3 : \boldsymbol{x} \in \mathcal{I}_{\boldsymbol{c}}\}$$

with

$$\mathcal{I}_{\boldsymbol{c}} := [-c_1/2, c_1/2] \times [-c_2/2, c_2/2] \times [-c_3/2, c_3/2]$$

are all of length β. Thus, the parallelepiped contains the ball of radius $\beta/2$. The Fourier space cutoff $\boldsymbol{M} \in 2\mathbb{N}^3$ is consequently chosen such that

$$\boldsymbol{M} \approx \boldsymbol{c} = (c_1, c_2, c_3), \tag{3.15}$$

i.e., we round to the next even integer in each component.

Remark 3.1. The conditions (3.14) are equivalent to

$$\frac{c_1}{\|\boldsymbol{\ell}_1\|} = \frac{c_2}{\|\boldsymbol{\ell}_2\|} = \frac{c_3}{\|\boldsymbol{\ell}_3\|} = \beta. \tag{3.16}$$

As an example, the vectors $\boldsymbol{n}_{23}$ and $\boldsymbol{\ell}_1$ are linearly dependent. Thus, we obtain

$$c_1\|\tilde{\boldsymbol{\ell}}_1\| \cdot |\cos \sphericalangle(\tilde{\boldsymbol{\ell}}_1, \boldsymbol{n}_{23})| = c_1\|\tilde{\boldsymbol{\ell}}_1\| \cdot |\cos \sphericalangle(\tilde{\boldsymbol{\ell}}_1, \boldsymbol{\ell}_1)| = c_1\frac{|\tilde{\boldsymbol{\ell}}_1 \cdot \boldsymbol{\ell}_1|}{\|\boldsymbol{\ell}_1\|} = \frac{c_1}{\|\boldsymbol{\ell}_1\|}.$$

□

Example 3.2. We consider a box spanned by the three vectors $\boldsymbol{\ell}_1 = (1, 0, 0)$, $\boldsymbol{\ell}_2 = (1, 1, 0)$ and $\boldsymbol{\ell}_3 = (0, 0, 1)$. The dual lattice vectors are given by $\tilde{\boldsymbol{\ell}}_1 = (1, -1, 0)$, $\tilde{\boldsymbol{\ell}}_2 = (0, 1, 0)$ and $\tilde{\boldsymbol{\ell}}_3 = (0, 0, 1)$. For $\beta := 8$ we obtain

$$\boldsymbol{c} = (8, 8\sqrt{2}, 8) \quad \text{and} \quad \boldsymbol{M} := (8, 12, 8),$$

which ensures

$$\{\boldsymbol{x} \in \mathbb{R}^3 : \|\boldsymbol{x}\| \le 4\} \subset \{x_1\tilde{\boldsymbol{\ell}}_1 + x_2\tilde{\boldsymbol{\ell}}_1 + x_3\tilde{\boldsymbol{\ell}}_1, \boldsymbol{x} \in \mathcal{I}_{\boldsymbol{c}}\}.$$

In contrast, for the lattice vectors $\boldsymbol{\ell}_1 = (1, 0, 0)$, $\boldsymbol{\ell}_2 = (0, 1, 0)$ and $\boldsymbol{\ell}_3 = (0, 0, 1)$ we obtain $\boldsymbol{M} = (8, 8, 8)$. For a graphical illustration in two dimensions see Figure 3.1. □

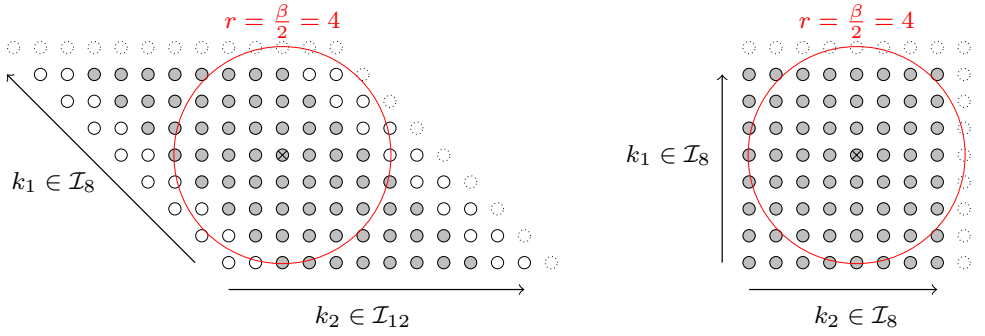

Figure 3.1: The sets $\{k_1\tilde{\boldsymbol{\ell}}_1 + k_2\tilde{\boldsymbol{\ell}}_2 : k_1 \in \mathcal{I}_{M_1}, k_2 \in \mathcal{I}_{M_2}\}$ for $\boldsymbol{\ell}_1 = (1,0)$, $\boldsymbol{\ell}_2 = (1,1)$ (left) and for $\boldsymbol{\ell}_1 = (1,0)$, $\boldsymbol{\ell}_2 = (0,1)$ (right).

Rms force errors for the charges

For the charges, i.e., $j = 1, \dots, N_\mathrm{c}$, we decompose the Fourier space part of the force $\boldsymbol{F}(j) = -q_j \nabla_{\boldsymbol{x}_j} \phi(j)$ via

$$\boldsymbol{F}^\mathrm{F}(j) = \boldsymbol{F}^\mathrm{F}_\mathrm{c.c.}(j) + \boldsymbol{F}^\mathrm{F}_\mathrm{c.d.}(j),$$

where

$$\begin{aligned}
\boldsymbol{F}^\mathrm{F}_\mathrm{c.c.}(j) &= -\frac{q_j \nabla_{\boldsymbol{x}_j}}{\pi V} \sum_{\boldsymbol{k} \in \mathbb{Z}^3} \hat{\psi}(\boldsymbol{k}) \sum_{i=1}^{N_\mathrm{c}} q_i \, \mathrm{e}^{2\pi \mathrm{i} \boldsymbol{k}^\top \boldsymbol{L}^{-1} \boldsymbol{x}_{ij}} = \frac{2\mathrm{i} q_j}{V} \sum_{i=1}^{N_\mathrm{c}} q_i \sum_{\boldsymbol{k} \in \mathbb{Z}^3} \hat{\psi}(\boldsymbol{k}) (\boldsymbol{L}^{-\top} \boldsymbol{k}) \, \mathrm{e}^{2\pi \mathrm{i} \boldsymbol{k}^\top \boldsymbol{L}^{-1} \boldsymbol{x}_{ij}}, \\
\boldsymbol{F}^\mathrm{F}_\mathrm{c.d.}(j) &= -\frac{q_j \nabla_{\boldsymbol{x}_j}}{\pi V} \sum_{\boldsymbol{k} \in \mathbb{Z}^3} \hat{\psi}(\boldsymbol{k}) \sum_{i=N_\mathrm{c}+1}^{N} \boldsymbol{\mu}_i^\top \nabla_{\boldsymbol{x}_i} \, \mathrm{e}^{2\pi \mathrm{i} \boldsymbol{k}^\top \boldsymbol{L}^{-1} \boldsymbol{x}_{ij}} \\
&= -\frac{4\pi q_j}{V} \sum_{i=N_\mathrm{c}+1}^{N} \|\boldsymbol{\mu}_i\| \sum_{\boldsymbol{k} \in \mathbb{Z}^3} \hat{\psi}(\boldsymbol{k}) \|\boldsymbol{L}^{-\top} \boldsymbol{k}\| \cos(\gamma_{i,\boldsymbol{k}}) (\boldsymbol{L}^{-\top} \boldsymbol{k}) \, \mathrm{e}^{2\pi \mathrm{i} \boldsymbol{k}^\top \boldsymbol{L}^{-1} \boldsymbol{x}_{ij}}, \qquad (3.17)
\end{aligned}$$

and $\gamma_{i,\boldsymbol{k}} := \sphericalangle(\boldsymbol{\mu}_i, \boldsymbol{L}^{-\top} \boldsymbol{k})$ denotes the angle between a lattice vector $\boldsymbol{L}^{-\top} \boldsymbol{k}$ and a dipole moment $\boldsymbol{\mu}_i$.

If the infinite sum is replaced by a finite sum over $\boldsymbol{k} \in \mathcal{I}_{\boldsymbol{M}}$, the Fourier space part $\boldsymbol{F}^\mathrm{F}_\mathrm{c.c.}(j)$ is approximated via

$$\boldsymbol{F}^\mathrm{F}_\mathrm{c.c.}(j) \approx \boldsymbol{F}^{\mathrm{F},\approx}_\mathrm{c.c.}(j) := \frac{2\mathrm{i} q_j}{V} \sum_{i=1}^{N_\mathrm{c}} q_i \sum_{\boldsymbol{k} \in \mathcal{I}_{\boldsymbol{M}}} \hat{\psi}(\boldsymbol{k}) (\boldsymbol{L}^{-\top} \boldsymbol{k}) \, \mathrm{e}^{2\pi \mathrm{i} \boldsymbol{k}^\top \boldsymbol{L}^{-1} \boldsymbol{x}_{ij}}$$

resulting in an error

$$\boldsymbol{F}^\mathrm{F}_\mathrm{c.c.}(j) - \boldsymbol{F}^{\mathrm{F},\approx}_\mathrm{c.c.}(j) = \sum_{i=1}^{N_\mathrm{c}} q_i \boldsymbol{\chi}(\boldsymbol{x}_{ij}),$$

where

$$\boldsymbol{\chi}(\boldsymbol{x}) := \frac{2\mathrm{i}}{V} \sum_{\boldsymbol{k} \in \mathbb{Z}^3 \setminus \mathcal{I}_{\boldsymbol{M}}} \hat{\psi}(\boldsymbol{k}) (\boldsymbol{L}^{-\top} \boldsymbol{k}) \, \mathrm{e}^{2\pi \mathrm{i} \boldsymbol{k}^\top \boldsymbol{L}^{-1} \boldsymbol{x}}.$$

Note that the rms force errors in the Fourier space part have already been computed in [27]. However, for the sake of completeness, we sketch the derivation of the error, following the common approach as presented and used in [9, 46], for instance. The result is slightly different from the one given in [27].

At first, we compute the quadratic mean

$$\chi^2 := \frac{1}{V} \int_{\boldsymbol{x} \in \boldsymbol{L}\mathbb{T}} \boldsymbol{\chi}(\boldsymbol{x})^\top \bar{\boldsymbol{\chi}}(\boldsymbol{x}) \, \mathrm{d}\boldsymbol{x} = \frac{4}{V^2} \sum_{\boldsymbol{k} \in \mathbb{Z}^3 \setminus \mathcal{I}_{\boldsymbol{M}}} \hat{\psi}(\boldsymbol{k})^2 \|\boldsymbol{L}^{-\top} \boldsymbol{k}\|^2 = \frac{4}{V^2} \sum_{\boldsymbol{k} \in \mathbb{Z}^3 \setminus \mathcal{I}_{\boldsymbol{M}}} \frac{\mathrm{e}^{-2\pi^2 \|\boldsymbol{L}^{-\top} \boldsymbol{k}\|^2 / \alpha^2}}{\|\boldsymbol{L}^{-\top} \boldsymbol{k}\|^2}$$

and we obtain, cf. [9, Eq. 19],

$$\begin{aligned}\left(\Delta F^{\mathrm{F}}_{\mathrm{c.c.}}\right)^2 &\approx \frac{Q^2}{N_{\mathrm{c}}}\chi^2 \approx \frac{4Q^2}{V^2 N_{\mathrm{c}}}\int_{\boldsymbol{k}\in\mathbb{Z}^3\setminus\mathcal{I}_{\boldsymbol{M}}} \frac{\mathrm{e}^{-2\pi^2\|\boldsymbol{L}^{-\top}\boldsymbol{k}\|^2/\alpha^2}}{\|\boldsymbol{L}^{-\top}\boldsymbol{k}\|^2}\mathrm{d}\boldsymbol{k} \\ &\leq \frac{4Q^2}{V^2 N_{\mathrm{c}}|\det(\boldsymbol{L}^{-\top})|}\int_{\|\boldsymbol{k}\|\geq\beta/2}\frac{\mathrm{e}^{-2\pi^2\|\boldsymbol{k}\|^2/\alpha^2}}{\|\boldsymbol{k}\|^2}\mathrm{d}\boldsymbol{k} \approx \frac{8\alpha^2Q^2}{\pi V N_{\mathrm{c}}\beta}\mathrm{e}^{-\pi^2\beta^2/2\alpha^2}\end{aligned}$$

or equivalently

$$\Delta F^{\mathrm{F}}_{\mathrm{c.c.}} \approx \alpha Q\sqrt{\frac{8}{\pi\beta N_{\mathrm{c}}V}}\mathrm{e}^{-\pi^2\beta^2/4\alpha^2}, \tag{3.18}$$

where we can replace $\beta = 3^{-1/2}\|\boldsymbol{L}^{-\top}\boldsymbol{M}\|$. Thereby, the infinite sum is approximated appropriately by an integral. The final result is obtained by using spherical coordinates as well as applying the asymptotic expansion of the complementary error function (3.6).

In the following we derive a proper estimate concerning the charge-dipole interaction, i.e., we estimate the rms error resulting from replacing the infinite sum in (3.17) by a sum over $\boldsymbol{k}\in\mathcal{I}_{\boldsymbol{M}}$. The integral, which has to be computed, contains $\cos^2(\gamma_{i,\boldsymbol{k}})$ for each i. Thus, the spherical coordinates are chosen such that $\theta = \gamma_{i,\boldsymbol{k}}$ for each i. We obtain

$$\begin{aligned}\delta F^{\mathrm{F}}_{\mathrm{c.d.}}(j)^2 &\approx \frac{16\pi^2 q_j^2}{V^2|\det(\boldsymbol{L}^{-\top})|}\sum_{i=N_{\mathrm{c}}+1}^{N}\|\boldsymbol{\mu}_i\|^2\int_0^{\pi}\sin(\theta)\cos^2(\theta)\mathrm{d}\theta\int_0^{2\pi}\mathrm{d}\phi\int_{\beta/2}^{\infty}\mathrm{e}^{-2\pi^2k^2/\alpha^2}k^2\mathrm{d}k \\ &= \frac{64\pi^3 q_j^2\mathcal{M}}{3V}\int_{\beta/2}^{\infty}\mathrm{e}^{-2\pi^2k^2/\alpha^2}k^2\mathrm{d}k \approx \frac{8\beta\alpha^2\pi q_j^2\mathcal{M}}{3V}\mathrm{e}^{-\pi^2\beta^2/2\alpha^2}\end{aligned}$$

and, finally,

$$\Delta F^{\mathrm{F}}_{\mathrm{c.d.}} := \sqrt{\frac{1}{N_{\mathrm{c}}}\sum_{j=1}^{N_{\mathrm{c}}}\delta F^{\mathrm{F}}_{\mathrm{c.d.}}(j)^2} \approx \alpha\sqrt{\frac{8\beta\pi Q\mathcal{M}}{3N_{\mathrm{c}}V}}\mathrm{e}^{-\pi^2\beta^2/4\alpha^2}. \tag{3.19}$$

Assuming that the contributions originating from interactions with charges and those resulting from interactions with dipoles are independent, we may approximate the rms far field error in the forces of the charges via

$$\Delta F^{\mathrm{F}}_{\mathrm{c}} \approx \sqrt{\left(\Delta F^{\mathrm{F}}_{\mathrm{c.c.}}\right)^2 + \left(\Delta F^{\mathrm{F}}_{\mathrm{c.d.}}\right)^2}. \tag{3.20}$$

Rms force errors for the dipole particles

For the dipoles, i.e., $j = N_{\mathrm{c}}+1,\ldots,N$, we can write the Fourier space part of the force as

$$\boldsymbol{F}^{\mathrm{F}}(j) = \boldsymbol{F}^{\mathrm{F}}_{\mathrm{d.c.}}(j) + \boldsymbol{F}^{\mathrm{F}}_{\mathrm{d.d.}}(j),$$

where

$$\begin{aligned}\boldsymbol{F}^{\mathrm{F}}_{\mathrm{d.c.}}(j) &= -\frac{\nabla_{\boldsymbol{x}_j}(\boldsymbol{\mu}_j^{\top}\nabla_{\boldsymbol{x}_j})}{\pi V}\sum_{\boldsymbol{k}\in\mathbb{Z}^3}\hat{\psi}(\boldsymbol{k})\sum_{i=1}^{N_{\mathrm{c}}}q_i\,\mathrm{e}^{2\pi\mathrm{i}\boldsymbol{k}^{\top}\boldsymbol{L}^{-1}\boldsymbol{x}_{ij}} \\ &= \frac{4\pi\|\boldsymbol{\mu}_j\|}{V}\sum_{i=1}^{N_{\mathrm{c}}}q_i\sum_{\boldsymbol{k}\in\mathbb{Z}^3}\hat{\psi}(\boldsymbol{k})\|\boldsymbol{L}^{-\top}\boldsymbol{k}\|\cos(\gamma_{j,\boldsymbol{k}})(\boldsymbol{L}^{-\top}\boldsymbol{k})\,\mathrm{e}^{2\pi\mathrm{i}\boldsymbol{k}^{\top}\boldsymbol{L}^{-1}\boldsymbol{x}_{ij}}, \\ \boldsymbol{F}^{\mathrm{F}}_{\mathrm{d.d.}}(j) &= -\frac{\nabla_{\boldsymbol{x}_j}(\boldsymbol{\mu}_j^{\top}\nabla_{\boldsymbol{x}_j})}{\pi V}\sum_{\boldsymbol{k}\in\mathbb{Z}^3}\hat{\psi}(\boldsymbol{k})\sum_{i=N_{\mathrm{c}}+1}^{N}\boldsymbol{\mu}_i^{\top}\nabla_{\boldsymbol{x}_i}\,\mathrm{e}^{2\pi\mathrm{i}\boldsymbol{k}^{\top}\boldsymbol{L}^{-1}\boldsymbol{x}_{ij}} \\ &= \frac{8\pi^2\mathrm{i}\|\boldsymbol{\mu}_j\|}{V}\sum_{i=N_{\mathrm{c}}+1}^{N}\|\boldsymbol{\mu}_i\|\sum_{\boldsymbol{k}\in\mathbb{Z}^3}\hat{\psi}(\boldsymbol{k})\|\boldsymbol{L}^{-\top}\boldsymbol{k}\|^2\cos(\gamma_{j,\boldsymbol{k}})\cos(\gamma_{i,\boldsymbol{k}})(\boldsymbol{L}^{-\top}\boldsymbol{k})\,\mathrm{e}^{2\pi\mathrm{i}\boldsymbol{k}^{\top}\boldsymbol{L}^{-1}\boldsymbol{x}_{ij}}.\end{aligned}$$

Analogously to the computation of $\Delta F^{\mathrm{F}}_{\mathrm{c.d.}}$, see (3.19), we obtain

$$\Delta F^{\mathrm{F}}_{\mathrm{d.c.}} \approx \alpha \sqrt{\frac{8\beta\pi Q\mathcal{M}}{3N_{\mathrm{d}}V}} \mathrm{e}^{-\pi^2\beta^2/4\alpha^2}. \tag{3.21}$$

In a similar fashion the error for dipole-dipole interactions is approximated. We finally obtain

$$\Delta F^{\mathrm{F}}_{\mathrm{d.d.}} \approx 4\alpha\mathcal{M} \sqrt{\frac{\pi^3\beta^3}{15N_{\mathrm{d}}V}} \mathrm{e}^{-\pi^2\beta^2/4\alpha^2}, \tag{3.22}$$

see [46, eq. (46)], where $k_c = \beta L/2$.

Assuming that the contributions originating from interactions with charges and those resulting from interactions with the other dipoles are independent, we may approximate the rms far field error in the forces of the dipoles via

$$\Delta F^{\mathrm{F}}_{\mathrm{d}} \approx \sqrt{\left(\Delta F^{\mathrm{F}}_{\mathrm{d.c.}}\right)^2 + \left(\Delta F^{\mathrm{F}}_{\mathrm{d.d.}}\right)^2}. \tag{3.23}$$

3.3 Summary

In this section we considered the estimation of the rms force errors resulting from truncating the Ewald formulas. Thereby, the short range as well as the long range parts are treated separately. In addition to the already known estimates for charge-charge and dipole-dipole interactions, see (3.7), (3.12), (3.18) and (3.22), we derived in an analog manner new estimates concerning the interactions between charges and dipoles, see (3.9), (3.11), (3.19) and (3.21). Provided that the different contributions to the approximation errors are independent from each other, the overall errors regarding the short range or rather the long range interactions may be approximated by (3.10) and (3.13) or rather (3.20) and (3.23), respectively. We emphasize that the estimates regarding the long range parts of the forces are valid for triclinic box structures, provided that the far field cutoff $\beta > 0$ is chosen large enough and such that (3.16) is fulfilled.

4 Fast evaluation of trigonometric sums for nonequispaced data

The well known fast Fourier transform enables the efficient evaluation of a trigonometric polynomial at N equispaced nodes with an arithmetic complexity of $\mathcal{O}(N \log N)$. In a wide range of applications an efficient sampling at nonequispaced knots is needed, which led to the development of the well known nonuniform FFT or rather fast Fourier transform for nonequispaced data (NFFT). In this section we give a short introduction to the NFFT and some of its variations that will be essential modules of our particle-mesh framework in Section 5. Thereby, we introduce two new NFFT variants called Hessian NFFT and adjoint gradient NFFT in Section 4.2.

4.1 The NFFT and available variants

The fast evaluation of a trigonometric polynomial

$$f(\boldsymbol{x}) = \sum_{\boldsymbol{k}\in\mathcal{I}_{\boldsymbol{M}}} \hat{f}_{\boldsymbol{k}}\, \mathrm{e}^{2\pi\mathrm{i}\boldsymbol{k}^{\top}\boldsymbol{x}} \tag{4.1}$$

at N given nodes $\boldsymbol{x}_j \in \mathbb{T}^3$, i.e., the fast computation of the sums

$$f(\boldsymbol{x}_j) = \sum_{\boldsymbol{k}\in\mathcal{I}_{\boldsymbol{M}}} \hat{f}_{\boldsymbol{k}}\, \mathrm{e}^{2\pi\mathrm{i}\boldsymbol{k}^{\top}\boldsymbol{x}_j} \tag{4.2}$$

for all $j = 1, \ldots, N$, is known as NFFT, [11, 3, 43, 10, 47, 42, 16, 24]. The idea is to map the arbitrarily spaced nodes $\boldsymbol{x}_j$ onto a regular grid via a so called window function φ (convolution),

since on a regular grid the transformation into spatial domain is possible based on the inverse FFT. In order to correct for the convolution with the window function φ the input coefficients $\hat{f}_{\boldsymbol{k}} \in \mathbb{C}$ can simply be divided by the Fourier coefficients $c_{\boldsymbol{k}}(\varphi)$ of the window function (deconvolution).

The usage of a larger grid of size $\boldsymbol{m} \geq \boldsymbol{M}$, where $\boldsymbol{m} \in 2\mathbb{N}^3$, can increase the accuracy of this approximate algorithm and is called oversampling. Thereby, we denote by

$$\sigma_j := \frac{m_j}{M_j} \geq 1, \ j \in \{1,2,3\}, \tag{4.3}$$

the oversampling factors of the single dimensions.

In summary, the NFFT algorithm consists of the following three steps.

i) Deconvolution in Fourier space:

$$\hat{g}_{\boldsymbol{k}} := \begin{cases} \frac{\hat{f}_{\boldsymbol{k}}}{c_{\boldsymbol{k}}(\tilde{\varphi})} & : \boldsymbol{k} \in \mathcal{I}_{\boldsymbol{M}}, \\ 0 & : \boldsymbol{k} \in \mathcal{I}_{\boldsymbol{m}} \setminus \mathcal{I}_{\boldsymbol{M}}. \end{cases}$$

ii) Inverse fast Fourier transform:

$$(\hat{g}_{\boldsymbol{k}})_{\boldsymbol{k} \in \mathcal{I}_{\boldsymbol{m}}} \mapsto (g_{\boldsymbol{l}})_{\boldsymbol{l} \in \mathcal{I}_{\boldsymbol{m}}}.$$

iii) Approximate the function values $f(\boldsymbol{x}_j)$ via

$$f(\boldsymbol{x}_j) \approx \sum_{\boldsymbol{l} \in \mathcal{I}_{\boldsymbol{m}}} g_{\boldsymbol{l}} \varphi\left(\boldsymbol{x}_j - \boldsymbol{l} \oslash \boldsymbol{m}\right), \tag{4.4}$$

where $\boldsymbol{l} \oslash \boldsymbol{m} := \left(\frac{l_1}{m_1}, \frac{l_2}{m_2}, \frac{l_3}{m_3}\right) \in \mathbb{R}^3$.

The described algorithm needs $\mathcal{O}(|\mathcal{I}_{\boldsymbol{m}}| \log |\mathcal{I}_{\boldsymbol{m}}| + N)$ arithmetic operations, whereas the direct evaluation of the sums (4.2) scales like $\mathcal{O}(|\mathcal{I}_{\boldsymbol{M}}| \cdot N)$. Increasing the support of the window function or choosing a higher resolution, i.e., increasing the oversampling rate, will reduce the resulting approximation errors. Some possible window functions will be introduced in Section 4.3. For recent considerations concerning error analysis for these window functions we refer to [30] and references therein. The following two variants of the NFFT are based on the same idea and thus yield the same arithmetic complexity.

Gradient NFFT

Consider again a trigonometric polynomial f as given in (4.1). We are now interested in the fast evaluation of the gradient ∇f at the given nodes $\boldsymbol{x}_j \in \mathbb{T}^3$, $j = 1, \ldots, N$. This can be done with a similar approximation as we use for the NFFT, see [38] for a detailed derivation. For the sake of brevity, we only give the resulting approximations.

If the differentiation is done in Fourier space, we obtain

$$\nabla f(\boldsymbol{x}_j) = 2\pi \mathrm{i} \sum_{\boldsymbol{k} \in \mathcal{I}_{\boldsymbol{M}}} \hat{f}_{\boldsymbol{k}} \, \mathrm{e}^{2\pi \mathrm{i} \boldsymbol{k}^{\top} \boldsymbol{x}_j} \boldsymbol{k} \quad \in \mathbb{C}^3, \tag{4.5}$$

i.e., the fast evaluation is possible via the NFFT in each of the three dimensions. This approach is widely known as i$\boldsymbol{k}$ differentiation.

Another variant is to apply the differentiation to the window function φ, i.e., the third step of the NFFT (4.4) is simply replaced by

$$\nabla f(\boldsymbol{x}_j) \approx \sum_{\boldsymbol{l} \in \mathcal{I}_{\boldsymbol{m}}} g_{\boldsymbol{l}} \nabla \varphi\left(\boldsymbol{x}_j - \boldsymbol{l} \oslash \boldsymbol{m}\right).$$

Note that this so called analytic differentiation approach only requires the computation of one inverse FFT of size $|\mathcal{I}_{\boldsymbol{m}}|$, whereas three inverse FFTs of the same size are needed for the i$\boldsymbol{k}$ differentiation approach.

Adjoint NFFT

The efficient computation of the sums

$$h(\boldsymbol{k}) = \sum_{j=1}^{N} f_j \, \mathrm{e}^{-2\pi \mathrm{i} \boldsymbol{k}^\top \boldsymbol{x}_j} \tag{4.6}$$

for all $\boldsymbol{k} \in \mathcal{I}_{\boldsymbol{M}}$, where the coefficients $f_j \in \mathbb{C}$, $j = 1, \ldots, N$, are given, is known as adjoint NFFT. Equation (4.2) can be written in matrix-vector form as

$$(f_j)_{j=1}^{N} = \boldsymbol{A} \left(\hat{f}_{\boldsymbol{k}} \right)_{\boldsymbol{k} \in \mathcal{I}_{\boldsymbol{M}}} \quad \text{with} \quad \boldsymbol{A} := \left(\mathrm{e}^{2\pi \mathrm{i} \boldsymbol{k}^\top \boldsymbol{x}_j} \right)_{j \in \{1,\ldots,N\}, \boldsymbol{k} \in \mathcal{I}_{\boldsymbol{M}}} \in \mathbb{C}^{N \times |\mathcal{I}_{\boldsymbol{M}}|}.$$

Thus, equation (4.6) reads as

$$\left(h(\boldsymbol{k}) \right)_{\boldsymbol{k} \in \mathcal{I}_{\boldsymbol{M}}} = \overline{\boldsymbol{A}}^\top (f_j)_{j=1}^{N}$$

with the adjoint matrix $\overline{\boldsymbol{A}}^\top$. The algorithm can be summarized as follows.

i) Convolution in spatial domain: For all $\boldsymbol{l} \in \mathcal{I}_{\boldsymbol{m}}$ compute

$$g_{\boldsymbol{l}} := \sum_{j=1}^{N} f_j \varphi \left(\boldsymbol{x}_j - \boldsymbol{l} \oslash \boldsymbol{m} \right). \tag{4.7}$$

ii) Fast Fourier transform:

$$(g_{\boldsymbol{l}})_{\boldsymbol{l} \in \mathcal{I}_{\boldsymbol{m}}} \mapsto (\hat{g}_{\boldsymbol{k}})_{\boldsymbol{k} \in \mathcal{I}_{\boldsymbol{m}}}. \tag{4.8}$$

iii) Deconvolution in Fourier space: For all $\boldsymbol{k} \in \mathcal{I}_{\boldsymbol{M}}$ approximate $h(\boldsymbol{k})$ via

$$h(\boldsymbol{k}) \approx \frac{\hat{g}_{\boldsymbol{k}}}{c_{\boldsymbol{k}}(\varphi)}. \tag{4.9}$$

4.2 Two new NFFT modules

In order to realize an efficient computation of the interactions with dipole particles, see Section 1, two new NFFT variants have been derived and implemented. The new variations, which we call Hessian NFFT and adjoint gradient NFFT, are of a great importance on their own and are shortly introduced in the following. Since the algorithms follow the same modular structure as the formerly derived NFFT variants, the same arithmetic complexity $\mathcal{O}(|\mathcal{I}_{\boldsymbol{m}}| \log |\mathcal{I}_{\boldsymbol{m}}| + N)$ is obtained.

Hessian NFFT

Similarly to the gradient NFFT, we are also able to evaluate the Hessian $\mathcal{H}f$ of a trigonometric polynomial f, see (4.1), at nonequispaced nodes $\boldsymbol{x}_j \in \mathbb{T}^3$, $j = 1, \ldots, N$. Differentiation in Fourier space gives

$$\mathcal{H}f(\boldsymbol{x}_j) = -4\pi^2 \sum_{\boldsymbol{k} \in \mathcal{I}_{\boldsymbol{M}}} \hat{f}_{\boldsymbol{k}} \, \mathrm{e}^{2\pi \mathrm{i} \boldsymbol{k}^\top \boldsymbol{x}_j} \boldsymbol{k}^\top \boldsymbol{k} \quad \in \mathbb{C}^{3\times 3}, \tag{4.10}$$

i.e., nine univariate NFFTs are required. Since $\mathcal{H}f(\boldsymbol{x}_j) \in \mathbb{C}^{3x3}$ is a symmetric matrix, we can reduce the computational effort to the computation of six one-dimensional NFFTs.

Applying the differentiation operators directly to the NFFT window function φ gives the analytic differentiation

$$\mathcal{H}f(\boldsymbol{x}_j) \approx \sum_{\boldsymbol{l} \in \mathcal{I}_{\boldsymbol{m}}} g_{\boldsymbol{l}} (\mathcal{H}\varphi) \left(\boldsymbol{x}_j - \boldsymbol{l} \oslash \boldsymbol{m} \right),$$

which replaces the convolution step (4.4) in the computation of the NFFT. Again, for the analytic differentiation approach only one inverse FFT of size $|\mathcal{I}_{\boldsymbol{m}}|$ has to be computed.

Adjoint gradient NFFT

The fast evaluation of

$$h(\boldsymbol{k}) = \sum_{j=1}^{N} \left(\boldsymbol{f}_j^\top \nabla_{\boldsymbol{x}}\right) \mathrm{e}^{-2\pi \mathrm{i} \boldsymbol{k}^\top \boldsymbol{x}}\Big|_{\boldsymbol{x}=\boldsymbol{x}_j} \quad \in \mathbb{C}, \tag{4.11}$$

for all $\boldsymbol{k} \in \mathcal{I}_{\boldsymbol{M}}$, where the nodes $\boldsymbol{x}_j \in \mathbb{T}^3$ as well as the vectors $\boldsymbol{f}_j \in \mathbb{C}^3$ are given, is called adjoint gradient NFFT. It can be computed via the adjoint NFFT as follows.

The i$\boldsymbol{k}$ differentiation approach gives

$$h(\boldsymbol{k}) = -2\pi \mathrm{i} \sum_{j=1}^{N} \boldsymbol{f}_j^\top \boldsymbol{k}\, \mathrm{e}^{-2\pi \mathrm{i} \boldsymbol{k}^\top \boldsymbol{x}_j} = -2\pi \mathrm{i} \left(\sum_{j=1}^{N} \boldsymbol{f}_j\, \mathrm{e}^{-2\pi \mathrm{i} \boldsymbol{k}^\top \boldsymbol{x}_j} \right)^\top \boldsymbol{k}.$$

Thus, we can compute a vector valued adjoint NFFT and then compute the scalar products with $\boldsymbol{k}$. For the analytic differentiation we replace the convolution step (4.7) in the adjoint NFFT by

$$g_{\boldsymbol{l}} := \sum_{j=1}^{N} \boldsymbol{f}_j^\top \nabla \varphi\left(\boldsymbol{x}_j - \boldsymbol{l} \oslash \boldsymbol{m}\right).$$

The FFT step (4.8) and deconvolution step (4.9) remain the same. Again, we stress that the analytic differentiation approach only needs one FFT, whereas the i$\boldsymbol{k}$ differentiation approach requires three FFTs.

4.3 Window functions

A variety of possible window functions φ has already been suggested in the literature. An overview on the available NFFT windows is given in [24], for instance. Note that in the scope of particle mesh methods B-splines are commonly used, cf. [19, 8, 7, 13, 6, 5]. But also for the Bessel window promising results have been achieved recently, see [30, 32]. Thus, the focus is set on the B-spline as well as the Bessel window function in this paper.

Note that the considered window functions are both compactly supported in spatial domain so that basically the same estimates for the resulting approximation errors are valid, see [43, 10, 42, 30, 38].

4.3.1 B-Spline window

The centered cardinal B-splines are defined recursively via

$$B_1(x) := \begin{cases} 1 & : x \in [-1/2, 1/2), \\ 0 & : \text{else}, \end{cases}$$
$$B_{n+1}(x) := (B_n * B_1)(x) \text{ for } n \in \mathbb{N},$$

where $*$ denotes the convolution operator on $\mathbb{R}$.

The NFFT window function is then chosen as, cf. [3, 41],

$$\varphi(\boldsymbol{x}) := B_{2p}(m_1 x_1) B_{2p}(m_2 x_2) B_{2p}(m_3 x_3)$$

via a tensor product approach, where we refer to $p \in \mathbb{N}$ as the support parameter. Thereby m_1, m_2, m_3 are the single components of the oversampled grid size $\boldsymbol{m}$. The window function is compactly supported with

$$\operatorname{supp}(\varphi) = [-p/m_1, p/m_1] \times [-p/m_2, p/m_2] \times [-p/m_3, p/m_3]. \tag{4.12}$$

The Fourier coefficients can be expressed in terms of the well known sinc function.

$$c_{\boldsymbol{k}}(\varphi) = \frac{1}{m_1 m_2 m_3} \operatorname{sinc}^{2p}\left(\tfrac{\pi k_1}{m_1}\right) \operatorname{sinc}^{2p}\left(\tfrac{\pi k_2}{m_2}\right) \operatorname{sinc}^{2p}\left(\tfrac{\pi k_3}{m_3}\right).$$

4.3.2 Bessel window

For some shape parameter $b > 0$ and $p \in \mathbb{N}$ we define

$$z(x) := \frac{1}{2} \begin{cases} I_0(b\sqrt{p^2 - x^2}) & : |x| \leq p, \\ 0 & : \text{else}, \end{cases}$$

see [23, 15, 21, 38], where I_0 denotes the modified zero-order Bessel function. In three dimensions we follow the tensor product approach in order to define the NFFT window function via

$$\varphi(\boldsymbol{x}) := z(m_1 x_1) z(m_2 x_2) z(m_3 x_3),$$

which is compactly supported with the support given in (4.12). Again, m_1, m_2, m_3 are the single components of the oversampled grid size $\boldsymbol{m}$. The Fourier coefficients can be expressed as

$$c_{\boldsymbol{k}}(\varphi) = \prod_{j=1}^{3} \frac{\sinh(p\sqrt{b^2 - 4\pi^2 k_j^2/m_j^2})}{m_j \sqrt{b^2 - 4\pi^2 k_j^2/m_j^2}},$$

where the square root gives one unit root for negative arguments, i.e., we have

$$\frac{\sinh(p\sqrt{b^2 - 4\pi^2 k_j^2/m_j^2})}{m_j \sqrt{b^2 - 4\pi^2 k_j^2/m_j^2}} = \frac{\sinh(\mathrm{i}\, p\sqrt{4\pi^2 k_j^2/m_j^2 - b^2})}{\mathrm{i}\, m_j \sqrt{4\pi^2 k_j^2/m_j^2 - b^2}} = \frac{\sin(p\sqrt{4\pi^2 k_j^2/m_j^2 - b^2})}{m_j \sqrt{4\pi^2 k_j^2/m_j^2 - b^2}}$$

if $b^2 - 4\pi^2 k_j^2/m_j^2 < 0$.

5 P^{2}NFFT for charges and dipoles

In the following we present a method for the efficient approximation of the potentials, fields and field gradients in charge-dipole systems. Based on the corresponding Ewald formulas the computation is basically split into a near field part, which is evaluated by direct summation, as well as a far field part, which is computed via the NFFT modules as presented in Section 4.

5.1 Computation of the potentials

As stated in Section 2, the Ewald formulas for the energy (1.1) have been derived in [29]. The Ewald representations for the potentials $\phi(j)$ follow immediately from that, see (2.1), (2.2) and (2.5). The self potentials for the charges as well as the self fields for the dipoles are obtained from (2.4) and the self potentials of the dipoles are equal to zero, since for $j \in \{N_\mathrm{c} + 1, \ldots, N\}$ we have

$$\phi^{\mathrm{self}}(j) = -\lim_{\boldsymbol{x} \to \boldsymbol{0}} \boldsymbol{\mu}_j^\top \nabla_{\boldsymbol{x}} \frac{\operatorname{erf}(\alpha \|\boldsymbol{x}\|)}{\|\boldsymbol{x}\|} = 0.$$

In summary, we obtain

$$\phi(j) = \phi^{\mathrm{short}}(j) + \phi^{\mathrm{F}}(j) - \phi^{\mathrm{self}}(j) + \phi^{\boldsymbol{0}}(j),$$

where

$$\phi^{\mathrm{short}}(j) := \sum_{i=1}^{N} {\sum_{\boldsymbol{n}\in\mathbb{Z}^3}}' \xi_i \frac{\operatorname{erfc}(\alpha\|\boldsymbol{x}_{ij}+\boldsymbol{L}\boldsymbol{n}\|)}{\|\boldsymbol{x}_{ij}+\boldsymbol{L}\boldsymbol{n}\|}, \tag{5.1}$$

$$\phi^{\mathrm{F}}(j) := \frac{1}{\pi V} \sum_{\boldsymbol{k}\in\mathbb{Z}^3} \hat{\psi}(\boldsymbol{k}) \left(\sum_{i=1}^{N} \xi_i \, \mathrm{e}^{2\pi\mathrm{i}\boldsymbol{k}^\top \boldsymbol{L}^{-1}\boldsymbol{x}_i} \right) \mathrm{e}^{-2\pi\mathrm{i}\boldsymbol{k}^\top \boldsymbol{L}^{-1}\boldsymbol{x}_j}, \tag{5.2}$$

$$\phi^{\mathrm{self}}(j) := \begin{cases} \frac{2\alpha}{\sqrt{\pi}} q_j & : j = 1,\dots,N_{\mathrm{c}}, \\ 0 & : j = N_{\mathrm{c}}+1,\dots,N, \end{cases}$$

$$\phi^{\boldsymbol{0}}(j) := \frac{4\pi}{3V} \left(\boldsymbol{D}_{\mathrm{c}}^\top \boldsymbol{x}_j - \frac{1}{2} \sum_{i=1}^{N_{\mathrm{c}}} q_i \|\boldsymbol{x}_i\|^2 - \sum_{i=N_{\mathrm{c}}+1}^{N} \boldsymbol{\mu}_i^\top \boldsymbol{x}_i + \boldsymbol{D}_{\mathrm{d}}^\top \boldsymbol{x}_j \right).$$

The computation of $\phi^{\mathrm{self}}(j)$ and $\phi^{\boldsymbol{0}}(j)$ is straightforward. Since the complementary error function $\operatorname{erfc}(\cdot)$ tends to zero exponentially fast, the short range parts of the potentials can be obtained via direct evaluation, e.g. via a so called linked cell method [19, Chap. 8.4], which is also available within the ScaFaCoS library [1]. Each particle interacts with a fixed number of neighbors, provided that the particles are distributed homogeneously. In this case the near field computations scale like $\mathcal{O}(N)$, where the constant depends on the applied near field cutoff radius r_{cut}.

The Fourier space parts $\phi^{\mathrm{F}}(j)$ are approximated as follows. Since the Fourier coefficients $\hat{\psi}(\boldsymbol{k})$, see (2.3), tend to zero exponentially fast in $\boldsymbol{k}$, the infinite sum over $\boldsymbol{k}\in\mathbb{Z}^3$ can be replaced by a sum involving all $\boldsymbol{k}\in\mathcal{I}_{\boldsymbol{M}}$, where $\boldsymbol{M}\in 2\mathbb{N}^3$ has to be chosen large enough.

Then, the structure factors can be written as

$$\begin{aligned} S(\boldsymbol{k}) &:= \sum_{i=1}^{N} \xi_i \, \mathrm{e}^{2\pi\mathrm{i}\boldsymbol{k}^\top \boldsymbol{L}^{-1}\boldsymbol{x}_i} \\ &= \sum_{i=1}^{N_{\mathrm{c}}} q_i \, \mathrm{e}^{2\pi\mathrm{i}\boldsymbol{k}^\top \boldsymbol{L}^{-1}\boldsymbol{x}_i} + \sum_{i=N_{\mathrm{c}}+1}^{N} \boldsymbol{\mu}_i^\top \nabla_{\boldsymbol{x}_i} \, \mathrm{e}^{2\pi\mathrm{i}\boldsymbol{k}^\top \boldsymbol{L}^{-1}\boldsymbol{x}_i} \\ &= \sum_{i=1}^{N_{\mathrm{c}}} q_i \, \mathrm{e}^{2\pi\mathrm{i}\boldsymbol{k}^\top \boldsymbol{L}^{-1}\boldsymbol{x}_i} + \sum_{i=N_{\mathrm{c}}+1}^{N} \boldsymbol{\mu}_i^\top \boldsymbol{L}^{-\top} \nabla_{\boldsymbol{x}} \, \mathrm{e}^{2\pi\mathrm{i}\boldsymbol{k}^\top \boldsymbol{x}} \Big|_{\boldsymbol{x}=\boldsymbol{L}^{-1}\boldsymbol{x}_i} =: S_{\mathrm{c}}(\boldsymbol{k}) + S_{\mathrm{d}}(\boldsymbol{k}), \end{aligned}$$

where $\boldsymbol{k}\in\mathcal{I}_{\boldsymbol{M}}$. In order to compute the structure factors of the charges $S_{\mathrm{c}}(\boldsymbol{k})$ we apply the adjoint NFFT, as introduced in Section 4.1, for the nodes $\boldsymbol{L}^{-1}\boldsymbol{x}_i\in\mathbb{T}^3$, $i=1,\dots,N_{\mathrm{c}}$. For the approximation of $S_{\mathrm{d}}(\boldsymbol{k})$ we can apply the adjoint gradient NFFT from Section 4.2, where we have to set $\boldsymbol{f}_i := \boldsymbol{L}^{-1}\boldsymbol{\mu}_i$, $i=N_{\mathrm{c}}+1,\dots,N$.

Finally, the Fourier space parts of the potentials

$$\phi^{\mathrm{F}}(j) \approx \frac{1}{\pi V} \sum_{\boldsymbol{k}\in\mathcal{I}_{\boldsymbol{M}}} \hat{\psi}(\boldsymbol{k}) S_{\approx}(\boldsymbol{k}) \, \mathrm{e}^{-2\pi\mathrm{i}\boldsymbol{k}^\top \boldsymbol{L}^{-1}\boldsymbol{x}_j}$$

are approximated via the NFFT. Thereby, we denote by $S_{\approx}(\boldsymbol{k})\approx S(\boldsymbol{k})$ the approximated structure factors obtained by the adjoint (gradient) NFFT, as described above.

5.2 Computation of the fields

The fields $\boldsymbol{E}(j) = -\nabla_{\boldsymbol{x}_j}\phi(j)$, $j=1,\dots,N$, can be written as

$$\boldsymbol{E}(j) = \boldsymbol{E}^{\mathrm{short}}(j) + \boldsymbol{E}^{\mathrm{F}}(j) - \boldsymbol{E}^{\mathrm{self}}(j) + \boldsymbol{E}^{\boldsymbol{0}}(j),$$

where

$$\boldsymbol{E}^{\mathrm{short}}(j) := -\nabla_{\boldsymbol{x}_j} \sum_{i=1}^{N} {\sum_{\boldsymbol{n}\in\mathbb{Z}^3}}' \xi_i \frac{\operatorname{erfc}(\alpha\|\boldsymbol{x}_{ij}+\boldsymbol{L}\boldsymbol{n}\|)}{\|\boldsymbol{x}_{ij}+\boldsymbol{L}\boldsymbol{n}\|}, \tag{5.3}$$

$$\boldsymbol{E}^{\mathrm{F}}(j) := -\frac{\nabla_{\boldsymbol{x}_j}}{\pi V} \sum_{\boldsymbol{k}\in\mathbb{Z}^3} \hat{\psi}(\boldsymbol{k}) S(\boldsymbol{k})\, \mathrm{e}^{-2\pi \mathrm{i}\boldsymbol{k}^{\top}\boldsymbol{L}^{-1}\boldsymbol{x}_j}, \tag{5.4}$$

$$\boldsymbol{E}^{\mathrm{self}}(j) := \begin{cases} \boldsymbol{0} & : j = 1,\dots,N_{\mathrm{c}}, \\ -\frac{4\alpha^3}{3\sqrt{\pi}}\boldsymbol{\mu}_j & : j = N_{\mathrm{c}}+1,\dots,N, \end{cases}$$

$$\boldsymbol{E}^{\boldsymbol{0}}(j) := -\frac{4\pi}{3V}\left(\boldsymbol{D}_{\mathrm{c}}+\boldsymbol{D}_{\mathrm{d}}\right).$$

Similarly to the computation of the potentials, the short range parts of the fields $\boldsymbol{E}^{\mathrm{short}}(j)$ can be obtained via a direct summation method.

Having approximated the sums $S(\boldsymbol{k})$ via the adjoint (gradient) NFFT, the outer sums can be evaluated via the gradient NFFT, cf. Section 4.1. If the i$\boldsymbol{k}$ differentiation approach is applied, we have

$$\boldsymbol{E}^{\mathrm{F}}(j) \approx \frac{2\mathrm{i}}{V}\boldsymbol{L}^{-\top} \sum_{\boldsymbol{k}\in\mathcal{I}_{\boldsymbol{M}}} \boldsymbol{k}\hat{\psi}(\boldsymbol{k}) S_{\approx}(\boldsymbol{k})\, \mathrm{e}^{-2\pi \mathrm{i}\boldsymbol{k}^{\top}\boldsymbol{L}^{-1}\boldsymbol{x}_j}.$$

In other words, we can apply the gradient NFFT for the nodes $\boldsymbol{L}^{-1}\boldsymbol{x}_j$ and multiply with $\boldsymbol{L}^{-\top}$ afterward, which is a simple consequence of the chain rule. The gradient NFFT with analytic differentiation can be applied analogously. Note that the availability of the gradient NFFT module makes it very easy to switch between the i$\boldsymbol{k}$ and analytic differentiation within this computation.

5.3 Computation of the field gradients

The negative field gradients $\boldsymbol{G}(j) = -\nabla_{\boldsymbol{x}_j}\nabla_{\boldsymbol{x}_j}^{\top}\phi(j)$, $j = 1,\dots,N$, can be written as

$$\boldsymbol{G}(j) = \boldsymbol{G}^{\mathrm{short}}(j) + \boldsymbol{G}^{\mathrm{F}}(j) - \boldsymbol{G}^{\mathrm{self}}(j),$$

where

$$\boldsymbol{G}^{\mathrm{short}}(j) := -\nabla_{\boldsymbol{x}_j}\nabla_{\boldsymbol{x}_j}^{\top} \sum_{i=1}^{N} {\sum_{\boldsymbol{n}\in\mathbb{Z}^3}}' \xi_i \frac{\operatorname{erfc}(\alpha\|\boldsymbol{x}_{ij}+\boldsymbol{L}\boldsymbol{n}\|)}{\|\boldsymbol{x}_{ij}+\boldsymbol{L}\boldsymbol{n}\|}, \tag{5.5}$$

$$\boldsymbol{G}^{\mathrm{F}}(j) := -\frac{\nabla_{\boldsymbol{x}_j}\nabla_{\boldsymbol{x}_j}^{\top}}{\pi V} \sum_{\boldsymbol{k}\in\mathbb{Z}^3} \hat{\psi}(\boldsymbol{k}) S(\boldsymbol{k})\, \mathrm{e}^{-2\pi \mathrm{i}\boldsymbol{k}^{\top}\boldsymbol{L}^{-1}\boldsymbol{x}_j}, \tag{5.6}$$

$$\boldsymbol{G}^{\mathrm{self}}(j) := \begin{cases} \frac{4\alpha^3}{3\sqrt{\pi}} q_j \boldsymbol{I}_{3,3} & : j = 1,\dots,N_{\mathrm{c}}, \\ \boldsymbol{0}_{3,3} & : j = N_{\mathrm{c}}+1,\dots,N. \end{cases}$$

Whereas the short range parts of the matrices $\boldsymbol{G}^{\mathrm{short}}(j)$ can be obtained via a direct evaluation, the Fourier space parts $\boldsymbol{G}^{\mathrm{F}}(j)$ are approximated with the Hessian NFFT, cf. Section 4.2. For the i$\boldsymbol{k}$ differentiation approach we get

$$\begin{aligned} \boldsymbol{G}^{\mathrm{F}}(j) &\approx \frac{4\pi}{V} \sum_{\boldsymbol{k}\in\mathcal{I}_{\boldsymbol{M}}} (\boldsymbol{L}^{-\top}\boldsymbol{k})(\boldsymbol{L}^{-\top}\boldsymbol{k})^{\top} \hat{\psi}(\boldsymbol{k}) S_{\approx}(\boldsymbol{k})\, \mathrm{e}^{-2\pi \mathrm{i}\boldsymbol{k}^{\top}\boldsymbol{L}^{-1}\boldsymbol{x}_j} \\ &= \frac{4\pi}{V}\boldsymbol{L}^{-\top} \left(\sum_{\boldsymbol{k}\in\mathcal{I}_{\boldsymbol{M}}} \boldsymbol{k}\boldsymbol{k}^{\top} \hat{\psi}(\boldsymbol{k}) S_{\approx}(\boldsymbol{k})\, \mathrm{e}^{-2\pi \mathrm{i}\boldsymbol{k}^{\top}\boldsymbol{L}^{-1}\boldsymbol{x}_j} \right) \boldsymbol{L}^{-1}. \end{aligned}$$

Thus, we apply the Hessian NFFT (4.10) for the nodes $\boldsymbol{L}^{-1}\boldsymbol{x}_j$ in order to compute the matrix valued sums. Following the chain rule, the obtained matrices have to be multiplied by $\boldsymbol{L}^{-\top}$ from

the left as well as by $\boldsymbol{L}^{-1}$ from the right. The gradient NFFT with analytic differentiation can be applied analogously. Again, the availability of the gradient NFFT module makes it very easy to switch between the i$\boldsymbol{k}$ and analytic differentiation.

5.4 Charged dipoles

The described method can also be easily used if charged dipoles are present. Consider a particle p at position $\boldsymbol{x}_p$, which has a charge q_p as well as a dipole moment $\boldsymbol{\mu}_p$. In other words, in this case we have

$$\xi_p = q_p + \boldsymbol{\mu}_p^\top \nabla_{\boldsymbol{x}_p}.$$

Thus, we may simply split the particle into two particles, namely a charge and a dipole, i.e., we set

$$\boldsymbol{x}_{j_1} := \boldsymbol{x}_p, q_{j_1} := q_p \quad \text{for some } j_1 \in \{1, \dots, N_\mathrm{c}\}$$

as well as

$$\boldsymbol{x}_{j_2} := \boldsymbol{x}_p, \boldsymbol{\mu}_{j_2} := \boldsymbol{\mu}_p \quad \text{for some } j_2 \in \{N_\mathrm{c}+1, \dots, N\}.$$

When computing the short range parts (5.1), (5.3) and (5.5) we simply have to avoid dividing by zero by ignoring zero distances. Furthermore, we have to pay attention to the self interactions between the two created particles concerning the Fourier space parts (5.2), (5.4) and (5.6), as described below.

The potential, the field as well as the field gradient of the two created particles will only differ by the self interaction terms, which are only subtracted for either the charge or the dipole, respectively. Thus, the potential of the charged dipole ϕ_p is given by the potential of the charge j_1, where the computed self interaction has already been removed, i.e., $\phi_p = \phi(j_1)$ or equivalently $\phi_p = \phi(j_2) - \frac{2\alpha}{\sqrt{\pi}} q_p$. Analogously, we obtain

$$\begin{aligned}
\boldsymbol{E}_p &= \boldsymbol{E}(j_2) = \boldsymbol{E}(j_1) + \tfrac{4\alpha^3}{3\sqrt{\pi}} \boldsymbol{\mu}_p, \\
\boldsymbol{G}_p &= \boldsymbol{G}(j_1) = \boldsymbol{G}(j_2) - \tfrac{4\alpha^3}{3\sqrt{\pi}} q_p \boldsymbol{I}_{3,3}.
\end{aligned}$$

Consequently, the energy is simply given by $U_p = q_p \phi_p - \boldsymbol{\mu}_p^\top \boldsymbol{E}_p$ and the overall force acting on the charged dipole is obtained via $\boldsymbol{F}_p = q_p \boldsymbol{E}_p + \boldsymbol{G}_p \boldsymbol{\mu}_p$.

6 Software and Implementation

As described above, we extended the implementation of the versatile P^{2}NFFT framework [40, 38] in order to treat systems containing both charges as well as dipoles. P^{2}NFFT is part of ScaFaCoS [1] – a massively parallel, open source software library for computing Coulomb interactions with various fast numerical methods, e.g. P^{3}M [19, 8, 9], FMM [17, 22], and multigrid based solvers [45, 4]. A detailed comparison of the methods available within ScaFaCoS was published in [2] and showed P^{2}NFFT to be the fastest method in most cases. We stress that P^{2}NFFT is a highly modularized framework. Therefore, adding support for charge-dipole and dipole-dipole interactions directly results in a variety of new particle-mesh methods that have not been implemented so far. Many particle-mesh methods can be interpreted as special cases of P^{2}NFFT by appropriate combination of modules. Recently, P^{2}NFFT has been extended to support any combination of periodic and non-periodic boundary conditions [33, 34] up to high precision. Therefore, our proposed algorithms also apply for mixed-periodic and open boundary conditions, although our numerical tests in this paper are restricted to the 3d-periodic case. In the following, we briefly describe the changes that were necessary in order to extend P^{2}NFFT to charge-dipole and dipole-dipole interactions.

Extension of the ScaFaCoS interface

The ScaFaCoS interface has been extended to dipole moment input vectors and the corresponding output vectors. For a given system the P^{2}NFFT computes

- the potentials $\phi(j)$ as well as the fields $\boldsymbol{E}(j)$ for all charges ($j = 1, \ldots, N_\mathrm{c}$),
- the fields $\boldsymbol{E}(j)$ and the negative field gradients $\boldsymbol{G}(j)$ for all dipoles ($j = N_\mathrm{c}+1, \ldots, N$).

Based on this, the energies per particle $U(j)$, the total energy U, the acting forces $\boldsymbol{F}(j)$ as well as the torques of the dipoles $\boldsymbol{\tau}(j)$ can be computed afterward with complexity $\mathcal{O}(N)$, see equations (1.4), (1.7), (1.5) and (1.6).

Near field computations

The computation of the near field interactions, see equations (5.1), (5.3) and (5.5), is directly delegated to the ScaFaCoS near field module. This module is shared among several solvers of ScaFaCoS and computes particle interactions with a given cutoff radius and a solver-specific short range function (e.g. based on the Ewald splitting). A linked cell scheme is used in order to compute the near field interactions efficiently. The massively parallel implementation is based on a parallel sorting library and dedicated data redistribution operations to implement the domain decomposition for Cartesian process grids and the creation of ghost particles, see [20]. The near field module supports triclinic box shapes and various types of periodic boundary conditions. It has been extended by introducing a separate type of dipole particles that are handled in the same way as the already existing charge particles, but with an additional solver-specific short range function to compute charge-dipole and dipole-dipole interactions.

Far field computations

The computation of the Fourier space sums, see equations (5.2), (5.4) and (5.6), is based on a variety of NFFT modules, see Sections 4 and 5. A massively parallel implementation of these modules is publicly available within the PNFFT software library [40, 36]. Motivated by the special needs of charge-dipole and dipole-dipole interactions we extended the PNFFT library with two modules for computing a Hessian NFFT (4.10) and the adjoint gradient NFFT (4.11). Following the modular approach of PNFFT, both new modules can be computed with various NFFT window functions, with analytic or Fourier space differentiation and with interlacing, cf. [38]. In addition, the PNFFT interface has been improved in order to support input and output vectors consisting of function values, gradients and Hessians. Note that the parallel algorithm of PNFFT is based on the PFFT framework [37, 35, 38] for computing massively parallel, fast Fourier transforms.

The PNFFT library also allows the direct evaluation of the various trigonometric sums. We refer to the direct computation of the sums (4.2) as discrete Fourier transform for nonequispaced data (NDFT), yielding an undesirable arithmetic complexity of $\mathcal{O}(N|\mathcal{I}_{\boldsymbol{M}}|)$. Note that this direct computation does not introduce approximation errors and, therefore, can be used as a reference method for numerical tests. Analogously, the sums (4.5), (4.10), (4.6) and (4.11) can be obtained via a direct evaluation, which we denote as gradient NDFT, the Hessian NDFT, the adjoint NDFT and the adjoint gradient NDFT, respectively. The P^{2}NFFT interface in ScaFaCoS enables the user to easily switch between the fast computation and the direct evaluation (via flag `pnfft_direct`).

Remark 6.1 (P^{2}NDFT Ewald)**.** By applying the direct evaluation methods (NDFT) instead of the fast modules (NFFT), the described method (P^{2}NFFT) is equivalent to a pure Ewald summation, where only the Ewald truncation errors, see Section 3, are present. Thus, we refer to this method as the P^{2}NDFT Ewald summation. This method can serve as a reference method for numerical experiments since its approximation error is well controllable by the error estimates in Section 7. □

Further features

We remark that the P^{2}NFFT method has already been generalized for the treatment of 2d- and 1d-periodic as well as open boundary conditions. This method follows the same modular process for all types of boundary conditions. In fact, a change of periodicity can be performed easily by replacing the Fourier coefficients $\hat{\psi}(\boldsymbol{k})$ with some appropriately precomputed coefficients, see [33, 34]. Note that the nature of the used Fourier coefficients is not relevant for the presented modifications for charge-dipole systems. Indeed, our modularized implementation already works for these cases. However, the numerical testing of the method under other types of periodic boundary conditions goes beyond the scope of this article and will be presented in a future work.

Furthermore, our implementation for computing charge-dipole interactions provides many more particle-mesh specific features including interlacing, analytic differentiation and differentiation in Fourier space, optimal influence functions in a P^{3}M like fashion and a variety of different window functions; cf. [38] for a detailed list of features and description of the framework.

7 Numerical examples

In this Section we present first numerical results. We start by verifying the derived truncation errors concerning the Ewald summation formulas by measuring the rms force errors of our P^{2}NDFT Ewald algorithm, which simply truncates the infinite lattice sums, cf. Remark 6.1. Next, we also present some results for the fast P^{2}NFFT algorithm, which show that the method can be tuned to high accuracy. We present results for the i$\boldsymbol{k}$ as well as for the analytic differentiation approach. Finally, we present two examples concerning runtime and complexity of the P^{2}NFFT method.

Example 7.1. We consider $N_\mathrm{c} = 50$ charges $q_j = (-1)^j$, $j = 1, \dots, N_\mathrm{c}$, as well as $N_\mathrm{d} = 50$ dipoles $\|\boldsymbol{\mu}_j\| = 1$, $j = N_\mathrm{c}+1, \dots, N$. The positions $\boldsymbol{x}_j$ are randomly distributed in a box spanned by the vectors $\boldsymbol{\ell}_1 = (10, 0, 0)$, $\boldsymbol{\ell}_2 = (0, 10, 0)$ and $\boldsymbol{\ell}_3 = (0, 0, 10)$, i.e., we consider a cubic box with volume $V = 10^3$. The dipole moments $\boldsymbol{\mu}_j$ are also randomly chosen as elements of $\{\boldsymbol{r} \in \mathbb{R}^3 : \|\boldsymbol{r}\| = 1\}$. Thus, we obtain $Q = \mathcal{M} = 50$ and the errors regarding charge-dipole and dipole-charge interactions are supposed to be of the same size, see (3.9) and (3.11) for the expected near field as well as (3.19) and (3.21) for the corresponding far field errors.

In Figure 7.1 we plot the expected rms force errors in the near field

- $\Delta F_{\mathrm{c.c.}}^{\mathrm{short}}$, see (3.7),
- $\Delta F_{\mathrm{c.d.}}^{\mathrm{short}} = \Delta F_{\mathrm{d.c.}}^{\mathrm{short}}$, see (3.9) and (3.11),
- $\Delta F_{\mathrm{d.d.}}^{\mathrm{short}}$, see (3.12),

as well as the expected far field errors

- $\Delta F_{\mathrm{c.c.}}^{\mathrm{F}}$, see (3.18),
- $\Delta F_{\mathrm{c.d.}}^{\mathrm{F}} = \Delta F_{\mathrm{d.c.}}^{\mathrm{F}}$, see (3.19) and (3.21),
- $\Delta F_{\mathrm{d.d.}}^{\mathrm{F}}$, see (3.22).

Thereby, we choose the cutoff radius in the near field $r_{\mathrm{cut}} = 6.0$ and the grid size is set to $\boldsymbol{M} = (48, 48, 48)$, according to the cubic box shape, and plot the predicted rms force errors for varying splitting parameters α.

We can see that all the expected errors are of a comparable size, which is far below the machine epsilon $\epsilon = 10^{-15}$, if we choose the splitting parameter $\alpha \approx 1.15$. Thus, we apply the P^{2}NDFT algorithm with this parameter combination in order to compute high accuracy reference data in the following examples. □

7.1 Verification of the Ewald truncation errors

In Section 3 we showed how the resulting rms errors in the forces can be predicted. The following numerical examples confirm the correctness of the derived error estimates.

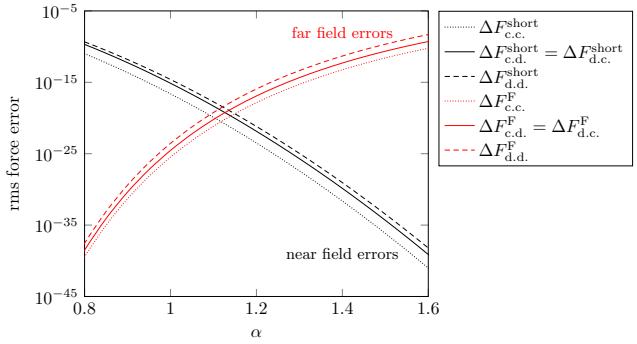

Figure 7.1: Predicted Ewald truncation errors in the forces for the above described test system with $N_{\text{c}} = 50$ charges and $N_{\text{d}} = 50$ dipoles. We plot the errors with respect to the splitting parameter α. The near field cutoff radius is set to $r_{\text{cut}} = 6.0$, the applied far field cutoff is $\boldsymbol{M} = (48, 48, 48)$.

Example 7.2. We compute the acting forces for a system of $N_{\text{c}} = 50$ randomly distributed charges with $|q_j| = 1$ as well as $N_{\text{d}} = 50$ randomly distributed dipoles with $\|\boldsymbol{\mu}_j\| = 1$ in the cubic box with edge length $L = 10$, see Example 7.1.

We apply the P^{2}NDFT method for different near field cutoffs $r_{\text{cut}} \in \{3.5, 4.0, 4.5, 5.0\}$ and far field cutoffs $\boldsymbol{M} = (M, M, M)$ with $M \in \{16, 24, 32\}$.

The reference data are computed via the P^{2}NDFT with $r_{\text{cut}} = 6.0$, $M = 48$ and $\alpha = 1.15$, see Example 7.1. The measured rms force errors, which match very well with the predicted errors, are plotted in Figure 7.2. □

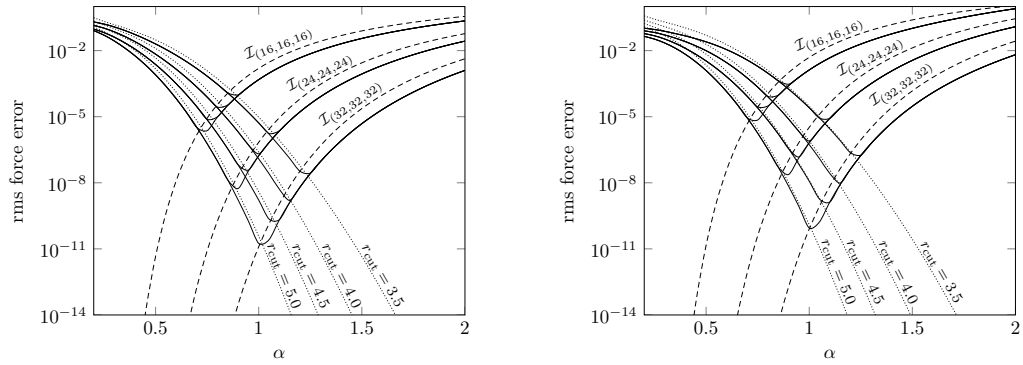

Figure 7.2: Predicted errors ΔF^{short} (dotted), see (3.10) and (3.13), and ΔF^{F} (dashed), see (3.20) and (3.23). The measured rms force errors are represented by the solid lines for the charges (left) as well as for the dipole particles (right). We use different near field as well as far field cutoffs (see labels).
Method: P^{2}NDFT, test system: random, cubic box, $N_{\text{c}} = N_{\text{d}} = 50$.

Example 7.3. We replace the cubic box spanned by the vectors $\boldsymbol{\ell}_1 = (10, 0, 0)$, $\boldsymbol{\ell}_2 = (0, 10, 0)$ and $\boldsymbol{\ell}_1 = (0, 0, 10)$ by a triclinic box spanned by

$$\boldsymbol{\ell}_1 = (10, 10, 0), \boldsymbol{\ell}_2 = (0, 10, 10) \text{ and } \boldsymbol{\ell}_1 = (0, 0, 10).$$

If the charges are appropriately mapped to the new box structure, the new particle systems is, under metallic boundary conditions, equivalent to the primary system in the cubic box, see Figure 7.3.

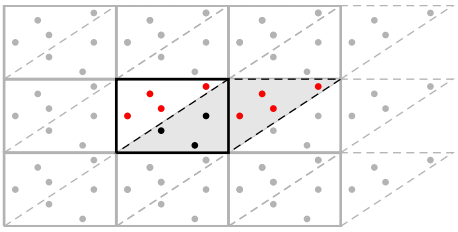

Figure 7.3: Particles distributed in a cubic box spanned by $\boldsymbol{\ell}_1 = (10, 0)$, $\boldsymbol{\ell}_2 = (0, 10)$ and equivalent particle system mapped to the triclinic box spanned by $\boldsymbol{\ell}_1 = (10, 10)$ and $\boldsymbol{\ell}_2 = (0, 10)$.

In order to verify the functionality of our algorithms for triclinic box shapes, we compute the reference data based on the equivalent cubic system as described in Example 7.1.

In Figure 7.4 we plot the predicted as well as the measured rms force errors for the triclinic particle system. Again, we use the P^{2}NDFT with different near field cutoffs $r_{\text{cut}} \in \{3.5, 4.0, 4.5, 5.0\}$ and different far field cutoffs

$$\boldsymbol{M} \approx \{10\sqrt{2}\beta, 10\sqrt{2}\beta, 10\beta\} \text{ with } \beta \in \{1.6, 2.4, 3.2\},$$

according to the lengths of the box vectors, cf. Equations (3.15) and (3.16). We can see that also for the triclinic particle systems the errors behave as expected. □

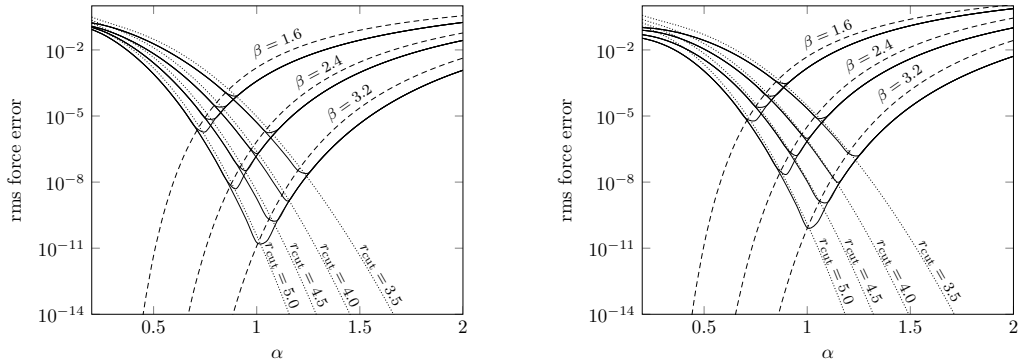

Figure 7.4: Predicted errors ΔF^{short} (dotted), see (3.10) and (3.13), and ΔF^{F} (dashed), see (3.20) and (3.23). The measured rms force errors are represented by the solid lines for the charges (left) as well as for the dipole particles (right). We use different near field as well as far field cutoffs (see legend).
Method: P^{2}NDFT, test system: random, triclinic box, $N_{\text{c}} = N_{\text{d}} = 50$.

7.2 Results for the P^{2}NFFT method

In this section we present numerical results for the fast NFFT based algorithm (P^{2}NFFT). As already mentioned above, we do not discuss the estimation of approximation errors introduced by the NFFT algorithms, since it goes beyond the scope of this article. However, the presented results show that the method computes the interactions correctly and can be tuned to a high precision.

We consider both, the i$\boldsymbol{k}$ as well as the analytic differentiation approach. In the case that oversampling is applied we use the same oversampling factor $\sigma = \sigma_1 = \sigma_2 = \sigma_3$ in all three dimensions, see (4.3). In our first examples we apply the B-spline as NFFT window function, which is widely used in the scope of particle mesh methods. In addition, we present results

obtained by using the Bessel window function, as introduced in Section 4.3.2. In comparison with the B-spline window, we can reduce the approximation errors significantly by using the Bessel window function, provided that the shape parameter b is chosen appropriately.

7.2.1 B-spline window

Example 7.4. We consider the same particle system as in Example 7.2. The trigonometric sums are now approximated via the NFFT algorithms as described in Section 5. Thereby we apply the B-spline of order 12, i.e., the support parameter is $p = 6$, as NFFT window function. We plot the obtained rms force errors with respect to the splitting parameter α in Figures 7.5 and 7.6. The reference data have been computed via the P^{2}NDFT Ewald method, as presented in Example 7.1.

In our tests we choose the near field cutoff radius $r_{\text{cut}} := 5$, apply different far field cutoffs $\boldsymbol{M} = (M, M, M)$, where $M \in \{16, 24, 32, 48\}$, as well as different oversampling factors $\sigma \in \{1, 1.25\}$.

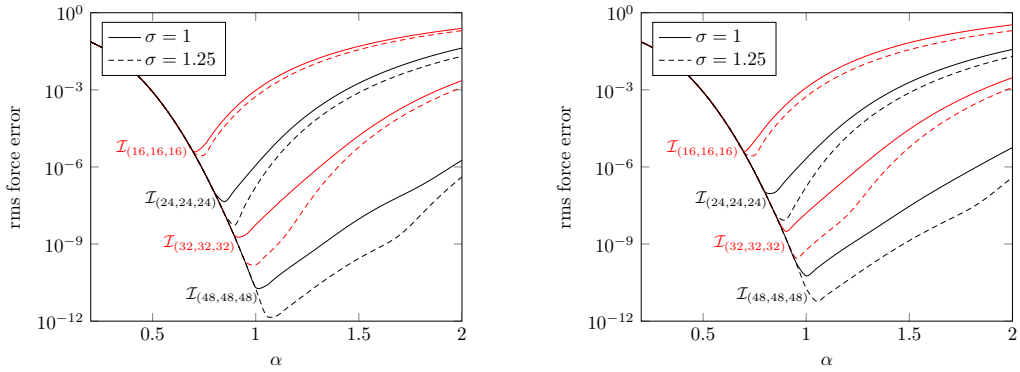

Figure 7.5: Rms force errors (3.1) for the charges. Applied parameters: near field cutoff $r_{\text{cut}} = 5$, different far field cutoffs $\boldsymbol{M} = (M, M, M)$ (see labels), B-spline window with support parameter $p = 6$, oversampling factor $\sigma = 1.0$ (solid) and $\sigma = 1.25$ (dashed), i$\boldsymbol{k}$-differentiation (left) and analytic differentiation (right).
Method: P^{2}NFFT, test system: random, cubic box, $N_{\text{c}} = N_{\text{d}} = 50$.

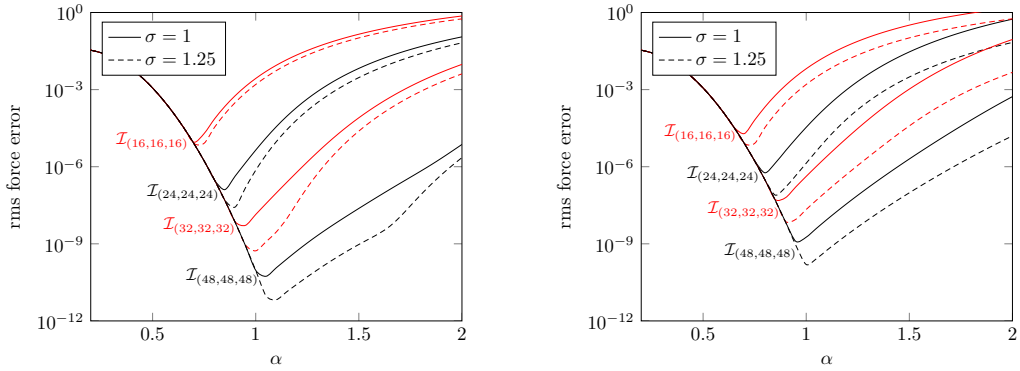

Figure 7.6: Rms force errors (3.2) for the dipoles. Applied parameters: near field cutoff $r_{\text{cut}} = 5$, different far field cutoffs $\boldsymbol{M} = (M, M, M)$ (see labels), B-spline window with support parameter $p = 6$, oversampling factor $\sigma = 1.0$ (solid) and $\sigma = 1.25$ (dashed), i$\boldsymbol{k}$-differentiation (left) and analytic differentiation (right). Method: P^{2}NFFT, test system: random, cubic box, $N_{\text{c}} = N_{\text{d}} = 50$.

□

Example 7.5. We consider the same triclinic particle system as in Example 7.3. The trigonometric sums are approximated via the NFFT algorithms with the same parameters as chosen in Example 7.4. We plot the obtained rms force errors with respect to the splitting parameter α in Figures 7.7 and 7.8. The reference data have been computed by considering the equivalent particle system in the cubic box via the P^{2}NDFT Ewald method, see Example 7.1.

According to the present triclinic box shape, we apply different far field cutoffs $\boldsymbol{M} = (10\sqrt{2}\beta, 10\sqrt{2}\beta, \beta)$, where $\beta \in \{1.6, 2.4, 3.2, 4.8\}$. □

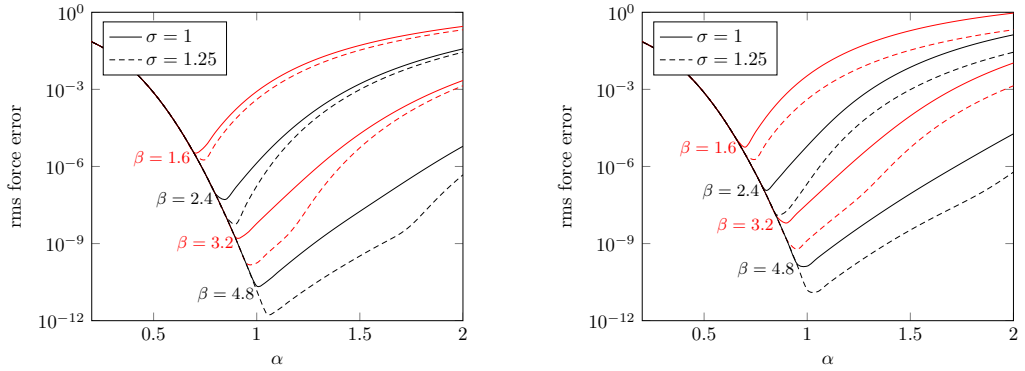

Figure 7.7: Rms force errors (3.1) for the charges. Applied parameters: near field cutoff $r_{\mathrm{cut}} = 5$, different far field cutoffs $\boldsymbol{M} \approx (10\sqrt{2}\beta, 10\sqrt{2}\beta, 10\beta)$ (see labels), B-spline window with support parameter $p = 6$, oversampling factor $\sigma = 1.0$ (solid) and $\sigma = 1.25$ (dashed), i$\boldsymbol{k}$-differentiation (left) and analytic differentiation (right).
Method: P^{2}NFFT, test system: random, triclinic box, $N_{\mathrm{c}} = N_{\mathrm{d}} = 50$.

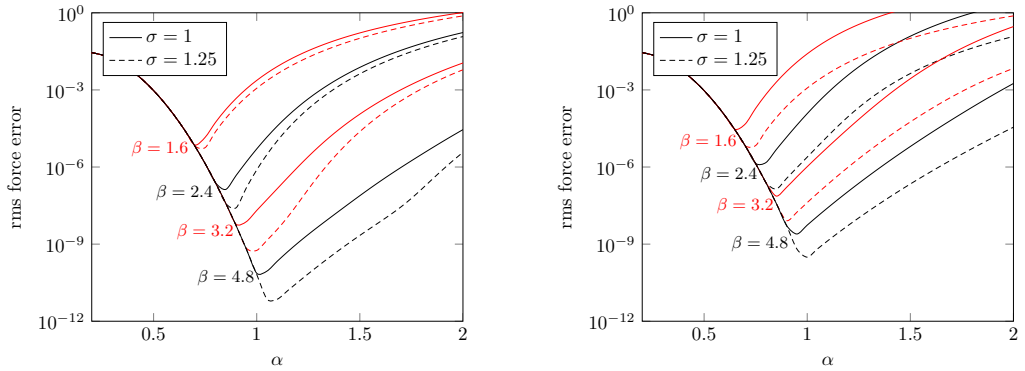

Figure 7.8: Rms force errors (3.2) for the dipoles. Applied parameters: near field cutoff $r_{\mathrm{cut}} = 5$, different far field cutoffs $\boldsymbol{M} \approx (10\sqrt{2}\beta, 10\sqrt{2}\beta, 10\beta)$ (see labels), B-spline window with support parameter $p = 6$, oversampling factor $\sigma = 1.0$ (solid) and $\sigma = 1.25$ (dashed), i$\boldsymbol{k}$-differentiation (left) and analytic differentiation (right).
Method: P^{2}NFFT, test system: random, triclinic box, $N_{\mathrm{c}} = N_{\mathrm{d}} = 50$.

7.2.2 Bessel window

In order to apply the Bessel window function, as introduced in Section 4.3.2, the support parameter b has to be chosen appropriately. It is already known that the choice of the shape parameter can influence the resulting approximation errors significantly. Especially in the case that the present Fourier coefficients are subject to a rapid decrease, a modification of the widely used standard value of b is necessary in order to tune the method to the best possible accuracy, see [30, 32].

Example 7.6. We consider the same particle system as in Examples 7.2 and 7.4. Now, we use the Bessel window function within the NFFT algorithms for varying shape parameter b and measure the resulting rms force errors. We optimized the shape parameter based on the measured errors via minimizing

$$\Delta F_{\mathrm{c}}^2 + \Delta F_{\mathrm{d}}^2$$

for each α. The optimal rms force errors, which have been achieved, are plotted in Figures 7.9 and 7.10. Some of the corresponding tuned shape parameters are shown in Figure 7.11. We can see that we can in some cases reduce the approximation errors significantly by using the Bessel window function with an appropriate shape parameter.

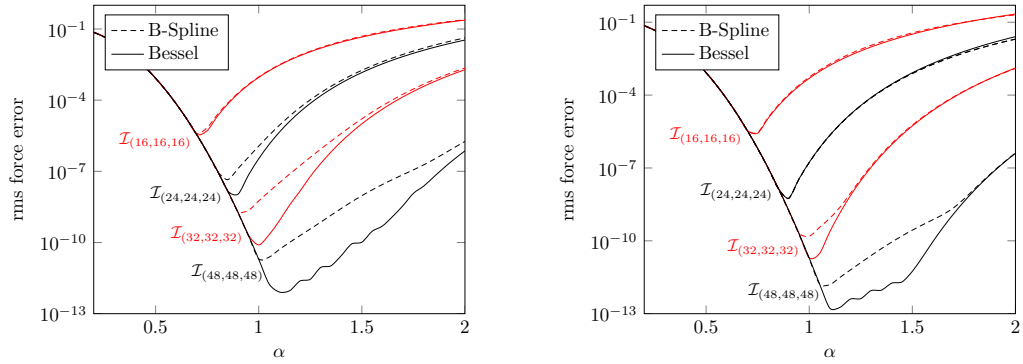

Figure 7.9: Rms force errors (3.1) for the charges compared for the Bessel and the B-spline window. Applied Parameters: near field cutoff $r_{\mathrm{cut}} = 5$, different far field cutoffs $\boldsymbol{M} = (M, M, M)$ (see labels), window support parameter $p = 6$, oversampling factor $\sigma = 1.0$ (left) and $\sigma = 1.25$ (right), i$\boldsymbol{k}$-differentiation approach.
Method: P^{2}NFFT, test system: random, cubic box, $N_{\mathrm{c}} = N_{\mathrm{d}} = 50$.

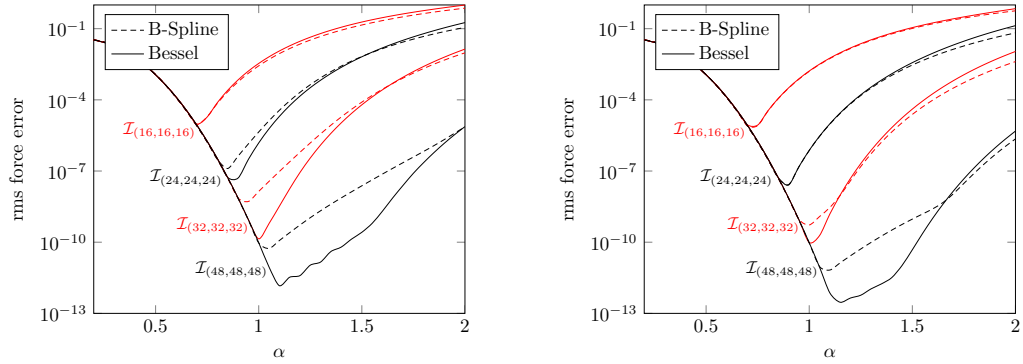

Figure 7.10: Rms force errors (3.2) for the dipoles compared for the Bessel and the B-spline window. Applied Parameters: near field cutoff $r_{\mathrm{cut}} = 5$, different far field cutoffs $\boldsymbol{M} = (M, M, M)$ (see labels), window support parameter $p = 6$, oversampling factor $\sigma = 1.0$ (left) and $\sigma = 1.25$ (right), i$\boldsymbol{k}$-differentiation approach.
Method: P^{2}NFFT, test system: random, cubic box, $N_{\mathrm{c}} = N_{\mathrm{d}} = 50$.

□

Example 7.7 (Accuracy and runtime)**.** We consider a particle system with $N_{\mathrm{c}} = 300$ charges with $|q_j| = 1$ and $N_{\mathrm{d}} = 300$ dipoles with $\|\boldsymbol{\mu}_j\| = 1$, randomly distributed in an orthorhombic box of size $20 \times 10 \times 10$. Based on the presented estimates for the Ewald truncation errors, see

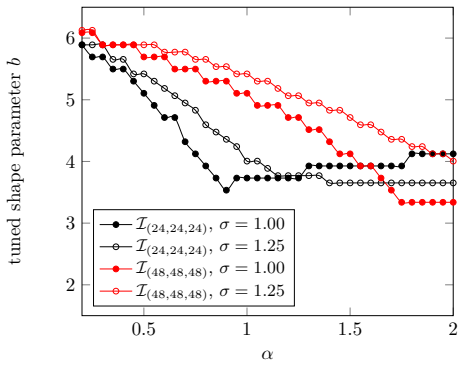

Figure 7.11: Tuned shape parameters b for the Bessel window function for some of the results presented in Figures 7.9 and 7.10.

Section 3, we may tune the shape parameter α and the far field cutoff β, in that order, for some given near field cutoff radius r_{cut} such that a certain accuracy ε is achieved.

In order to achieve the same accuracy ε with our fast NFFT based algorithms, the NFFT parameters have to be chosen such that the introduced approximation errors are sufficiently small. We remark that we have not derived according error estimates in the present work. This is subject of ongoing research. Thus, we compute accurate reference data based on the P^2NDFT Ewald method, as already done in the previously considered examples, and measure the resulting rms force errors.

Note that the accuracy of all NFFT variants is controlled by the support parameter p and the oversampling factor σ. Enlarging p or σ will result in a higher accuracy, as already stated in Section 4.1. One combination of p and σ is expected to be optimal regarding runtime for a fixed accuracy. In this Example we set $\varepsilon := 10^{-5}$ and consider different combinations of the support parameter p and oversampling factor σ. For each near field cutoff radius we keep the combination with the minimal computation time amongst all combinations yielding an accuracy of at least $\varepsilon = 10^{-5}$. In order to compute the required partial derivatives we apply the i$\boldsymbol{k}$ differentiation approach. For simplicity we restrict our considerations to the B-spline window function. In case of the Bessel window the shape parameter b will be an additional parameter influencing the accuracy.

In Figure 7.12 we plot the measured runtimes with respect to r_{cut} as well as the achieved rms force errors. The tuned parameters α and β as well as the optimal values for p and σ are presented separately. Among all considered parameter sets the one for $r_{\text{cut}} = 5.7$ is optimal regarding the required computational cost. We emphasize that this strongly depends on the used software and hardware. The runtime measurements for this example have been performed on an Intel i5-3470 processor that runs on 3.20 GHz with 8 GB main memory. Furthermore, the time needed for the computation of the FFTs very much depends on whether the oversampled mesh size $\boldsymbol{m}$ yields an advantageous decomposition into prime factors. Thus, single plots may yield unexpected behavior or rather jumps. □

We claim that the parameters, once tuned for a small particle system, can be applied to larger particle systems, provided that the charge as well as the dipole densities are kept almost constant, see Example 7.8. This has already been successfully applied in numerical experiments concerning charge-charge interactions, see [32] and references therein.

Example 7.8 (Complexity)**.** In the following numerical test we consider larger particle systems with the same particle density, where the number of particles as well as the volume of the box is increased by the factor 4, step by step. All particle systems consist of $N_{\text{c}} = N/2$ charges with $|q_j| = 1$ as well as $N_{\text{d}} = N/2$ dipoles with $\|\boldsymbol{\mu}_j\| = 1$, randomly distributed in an orthorhombic box of size $L_1 \times L_2 \times L_3$, as summarized in the table in Figure 7.13. The following parameters

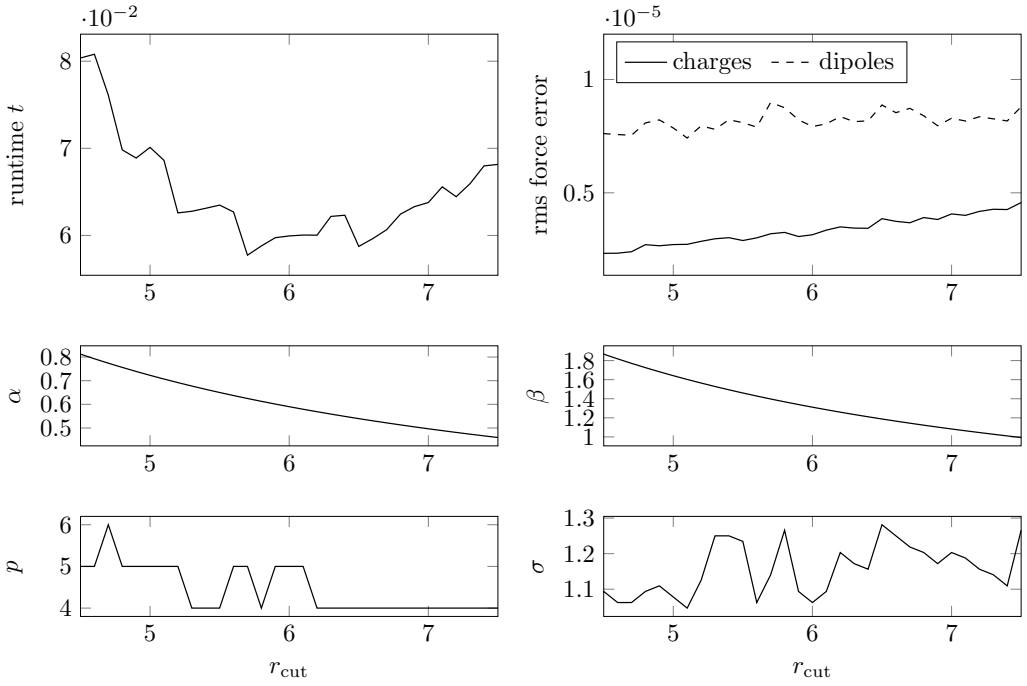

Figure 7.12: Required runtimes, achieved rms force errors and tuned parameters. The required accuracy was set to $\varepsilon = 10^{-5}$. Method: P^{2}NFFT with B-spline window. Test system: random, orthorhombic box of size $20 \times 10 \times 10$, $N_\mathrm{c} = N_\mathrm{d} = 300$.

turned out to be optimal in case of the small particle system: near field cutoff radius $r_\mathrm{cut} \approx 5.7$, splitting parameter $\alpha \approx 0.62$, far field cutoff $\beta \approx 1.4$, support parameter $p = 5$, oversampling factor $\sigma \approx 1.15$. The same parameters are now applied to the considered larger particle systems. For demonstrational purposes, we compute reference data of a higher accuracy and measure the resulting rms force errors also for the large particle systems. We achieve almost constant errors among all considered systems, see Figure 7.13. Note that keeping β and σ constant results in a linear scaling of the FFT size with the number of particles N, i.e., an $\mathcal{O}(N \log N)$ scaling is achieved regarding the far field computations. Since the near field cutoff r_cut is kept constant, the near field computations scale like $\mathcal{O}(N)$. In summary, we end up with an arithmetic complexity of $\mathcal{O}(N \log N)$. We expect that a further optimization with respect to runtime, applied for each of the considered systems, will even yield an arithmetic complexity of $\mathcal{O}(N\sqrt{\log N})$, cf. [38, Section 4.8].

□

8 Summary

In the present paper we propose an approach for the efficient evaluation of the interactions in electrostatic systems containing charges as well as dipoles. Therewith, we present for the first time an $\mathcal{O}(N \log N)$ algorithm capable of approximating electrostatic interactions in charge-dipole systems. The method is based on the well known Ewald summation technique. An error control concerning the truncation of the Ewald sums is possible based on estimating the root mean square errors in the forces, for instance. Analogously to the well known error estimates for charge-charge as well as dipole-dipole interactions under 3d-periodic boundary conditions, we derived new estimates for mixed particle systems, which have been verified by numerical examples.

An efficient evaluation of the energies as well as the acting forces, for instance, is realized based

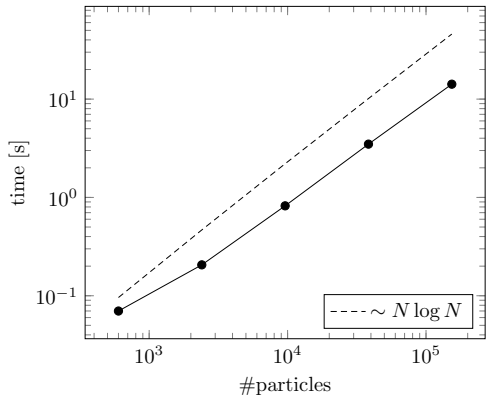

N	L_1	L_2	L_3	ΔF_c	ΔF_d
600	20	10	10	3.19e–6	8.99e–6
2400	20	20	20	3.19e–6	8.20e–6
9600	40	40	20	3.19e–6	8.41e–6
38400	80	40	40	3.21e–6	8.38e–6
153600	80	80	80	3.22e–6	8.40e–6

Figure 7.13: Measured computation times, where the mesh size scales linearly with the number of particles (left). Details concerning the considered particle systems and the measured rms force errors can be found in the table on the right hand side.

on the FFT for nonequispaced data, since the particle positions are arbitrarily distributed in a primary box. In order to compute the interactions to the dipole particles, new modules of the NFFT, namely the Hessian NFFT as well as the adjoint gradient NFFT, have been derived and implemented. The presented approach is an extension of the P^{2}NFFT method, which becomes now applicable to an even wider range of possible applications. The method is publicly available as a part of the ScaFaCoS library. All implemented modules of the NFFT, namely the adjoint NFFT, the gradient NFFT, the Hessian NFFT as well as the adjoint gradient NFFT, which may also be interesting for other applications, are also publicly available via the PNFFT library, which is used within the P^{2}NFFT method. For all modules, which require the computation of derivatives, the i$\boldsymbol{k}$ as well as the analytic differentiation approach are applicable. Note that the application of the fast NFFT modules introduce further approximation errors, which have not been considered here. An extended analysis of the resulting NFFT approximation errors is subject to future research. The library additionally enables a direct or rather exact computation of the considered trigonometric sums, which we refer to as the NDFT. Using the NDFT instead of the NFFT modules within our algorithms yields a pure Ewald summation reference method, which we call P^{2}NDFT Ewald. The errors of this method are well controllable via the presented Ewald truncation errors, as already mentioned above.

Our numerical results show that the P^{2}NFFT method for charge-dipole systems can be tuned to a high precision. We obtain very exact approximations when using analytic differentiation as well as in the case that i$\boldsymbol{k}$ differentiation is applied. As an NFFT window function we compared the widely used B-spline window as well as the Bessel window. The numerical results show that if the shape parameter of the Bessel function is chosen appropriately, the resulting approximation errors are in many cases significantly smaller than for the B-spline window. In this paper we concentrated on the 3d-periodic case, where we also considered triclinic box shapes. We remark that an error analysis regarding the approximation errors resulting from applying the fast NFFT modules as well as the derivation of an appropriate automated parameter tuning are subject of ongoing research. However, via tuning all involved parameters based on measuring the runtimes as well as the resulting approximation errors for a small particle systems, the proposed $\mathcal{O}(N \log N)$ scaling was verified in the present work.

We emphasize that the P^{2}NFFT method has already been implemented for 2d-periodic, 1d-periodic as well as for open boundary conditions. In the 3d-periodic case the underlying Fourier coefficients are known analytically. For all other types of periodic boundary conditions we simply replace these Fourier coefficients by some appropriately precomputed coefficients, which has already been tested for pure charge systems. We can proceed analogously for systems, where also dipole particles are present. In other words, the presented algorithms already work for all types of

periodic boundary conditions and our implementation within the ScaFaCoS library supports these cases. Numerical results for other boundary conditions will be presented elsewhere. Analogously to the charge-charge case the proposed charge-dipole method is built on top of the same optimized modules of the PNFFT [40, 36] and PFFT [37, 35] software libraries and can be assumed to yield the same performance on massively parallel architectures, cf. [37, 40, 2].

Acknowledgments

F. Nestler gratefully acknowledges support by the German Research Foundation (DFG), project PO 711/12-1. Furthermore, F. Nestler thanks Prof. C. Holm as well as the members of his working group, especially R. Weeber and F. Weik, for the invitation to the ICP Stuttgart and for fruitful discussions.

References

[1] A. Arnold, M. Bolten, H. Dachsel, F. Fahrenberger, F. Gähler, R. Halver, F. Heber, M. Hofmann, J. Iseringhausen, I. Kabadshow, O. Lenz, and M. Pippig: *ScaFaCoS - Scalable Fast Coloumb Solvers*. http://www.scafacos.de.

[2] A. Arnold, F. Fahrenberger, C. Holm, O. Lenz, M. Bolten, H. Dachsel, R. Halver, I. Kabadshow, F. Gähler, F. Heber, J. Iseringhausen, M. Hofmann, M. Pippig, D. Potts, and G. Sutmann: *Comparison of scalable fast methods for long-range interactions.* Phys. Rev. E, 88:063308, 2013.

[3] G. Beylkin: *On the fast Fourier transform of functions with singularities.* Appl. Comput. Harmon. Anal., 2:363–381, 1995.

[4] M. Bolten: *Multigrid methods for structured grids and their application in particle simulation.* PhD thesis, Bergische Universität Wuppertal, Wuppertal, 2008.

[5] J.J. Cerdà, V. Ballenegger, and C. Holm: *Particle-particle particle-mesh method for dipolar interactions: On error estimates and efficiency of schemes with analytical differentiation and mesh interlacing.* J. Chem. Phys., 135:184110, 2011.

[6] J.J. Cerdà, V. Ballenegger, O. Lenz, and C. Holm: *P3M algorithm for dipolar interactions.* J. Chem. Phys., 129:234104, 2008.

[7] T. Darden, D. York, and L. Pedersen: *Particle mesh Ewald: An $n\log(n)$ method for Ewald sums in large systems.* J. Chem. Phys., 98:10089–10092, 1993.

[8] M. Deserno and C. Holm: *How to mesh up Ewald sums. I. A theoretical and numerical comparison of various particle mesh routines.* J. Chem. Phys., 109:7678–7693, 1998.

[9] M. Deserno and C. Holm: *How to mesh up Ewald sums. II. An accurate error estimate for the Particle-Particle-Particle-Mesh algorithm.* J. Chem. Phys., 109:7694–7701, 1998.

[10] A.J.W. Duijndam and M.A. Schonewille: *Nonuniform fast Fourier transform.* Geophysics, 64:539–551, 1999.

[11] A. Dutt and V. Rokhlin: *Fast Fourier transforms for nonequispaced data.* SIAM J. Sci. Stat. Comput., 14:1368–1393, 1993.

[12] J. Eastwood, R. Hockney, and D. Lawrence: *P3M3DP—The three-dimensional periodic particle-particle/ particle-mesh program.* Computer Physics Communications, 19(2):215 – 261, 1980, ISSN 0010-4655.

[13] U. Essmann, L. Perera, M.L. Berkowitz, T. Darden, H. Lee, and L.G. Pedersen: *A smooth particle mesh Ewald method.* J. Chem. Phys., 103:8577–8593, 1995.

[14] P.P. Ewald: *Die Berechnung optischer und elektrostatischer Gitterpotentiale.* Ann. Phys., 369:253–287, 1921.

[15] K. Fourmont: *Non equispaced fast Fourier transforms with applications to tomography.* J. Fourier Anal. Appl., 9:431–450, 2003.

[16] L. Greengard and J.Y. Lee: *Accelerating the nonuniform fast Fourier transform.* SIAM Rev., 46:443–454, 2004.

[17] L. Greengard and V. Rokhlin: *A fast algorithm for particle simulations.* J. Comput. Phys., 73:325–348, 1987.

[18] F. Hedman and A. Laaksonen: *Ewald summation based on nonuniform fast Fourier transform.* Chem. Phys. Lett., 425:142–147, 2006.

[19] R.W. Hockney and J.W. Eastwood: *Computer simulation using particles.* Taylor & Francis, Inc., Bristol, PA, USA, 1988.

[20] M. Hofmann and G. Rünger: *Efficient Data Redistribution Methods for Coupled Parallel Particle Codes.* In *Proc. of the 42nd International Conference on Parallel Processing (ICPP-2013)*, pp. 40–49. IEEE, 2013.

[21] J.I. Jackson, C.H. Meyer, D.G. Nishimura, and A. Macovski: *Selection of a convolution function for Fourier inversion using gridding.* IEEE Trans. Med. Imag., 10:473–478, 1991.

[22] I. Kabadshow: *Periodic Boundary Conditions and the Error-Controlled Fast Multipole Method.* PhD thesis, Bergische Universität Wuppertal, Jülich, 2012.

[23] J.F. Kaiser: *Digital filters.* In F.F. Kuo and J.F. Kaiser (eds.): *System analysis by digital computer.* Wiley, New York, 1966.

[24] J. Keiner, S. Kunis, and D. Potts: *Using NFFT3 - a software library for various nonequispaced fast Fourier transforms.* ACM Trans. Math. Software, 36:Article 19, 1–30, 2009.

[25] V. Khoromskaia and B.N. Khoromskij: *Fast tensor method for summation of long-range potentials on 3D lattices with defects.* Numer. Linear Algebra Appl., 23:249–271, 2016, ISSN 1070-5325.

[26] L. af Klinteberg, D.S. Shamshirgar, and A.K. Tornberg: *Fast Ewald summation for free-space Stokes potentials.* ArXiv e-prints, 2016. arXiv:1607.04808v1 [math.NA].

[27] J. Kolafa and J.W. Perram: *Cutoff errors in the Ewald summation formulae for point charge systems.* Mol. Simul., 9(5):351–368, 1992.

[28] S.W. de Leeuw, J.W. Perram, and E.R. Smith: *Simulation of electrostatic systems in periodic boundary conditions. I. Lattice sums and dielectric constants.* Proc. R. Soc. Lond. Ser. A Math. Phys. Eng. Sci., 373:27–56, 1980.

[29] S.W. de Leeuw, J.W. Perram, and E.R. Smith: *Simulation of electrostatic systems in periodic boundary conditions. I. Lattice sums and dielectric constants.* Proc. Roy. Soc. London Ser. A, 373:27–56, 1980.

[30] F. Nestler: *Automated parameter tuning based on RMS errors for nonequispaced FFTs.* Adv. Comput. Math., 42(4):889–919, 2016.

[31] F. Nestler: *An NFFT based approach to the efficient computation of dipole–dipole interactions under various periodic boundary conditions.* Appl. Numer. Math., 105:25 – 46, 2016.

[32] F. Nestler: *Parameter tuning for the NFFT based fast Ewald summation.* Front. Phys., 4(28), 2016, ISSN 2296-424X.

[33] F. Nestler, M. Pippig, and D. Potts: *Fast Ewald summation based on NFFT with mixed periodicity.* J. Comput. Phys., 285:280–315, 2015.

[34] F. Nestler, M. Pippig, and D. Potts: *NFFT based fast Ewald summation for various types of periodic boundary conditions.* In G. Sutmann, J. Grotendorst, G. Gompper, and D. Marx (eds.): *Computational Trends in Solvation and Transport in Liquids*, vol. 28 of *IAS-Series*, pp. 575–598, Jülich, 2015. Forschungszentrum Jülich GmbH.

[35] M. Pippig: *PFFT - Parallel FFT software library.* https://github.com/mpip/pfft.

[36] M. Pippig: *PNFFT - Parallel Nonequispaced FFT software library.* https://github.com/mpip/pnfft.

[37] M. Pippig: *PFFT - An extension of FFTW to massively parallel architectures.* SIAM J. Sci. Comput., 35:C213–C236, 2013.

[38] M. Pippig: *Massively Parallel, Fast Fourier Transforms and Particle-Mesh Methods.* Dissertation. Universitätsverlag Chemnitz, 2015, ISBN 978-3-944640-76-1.

[39] M. Pippig and D. Potts: *Particle simulation based on nonequispaced fast Fourier transforms.* In G. Sutmann, P. Gibbon, and T. Lippert (eds.): *Fast Methods for Long-Range Interactions in Complex Systems*, vol. 6 of *IAS-Series*, pp. 131–158, Jülich, 2011. Forschungszentrum Jülich GmbH.

[40] M. Pippig and D. Potts: *Parallel three-dimensional nonequispaced fast Fourier transforms and their application to particle simulation.* SIAM J. Sci. Comput., 35:C411–C437, 2013.

[41] D. Potts and G. Steidl: *Fast summation at nonequispaced knots by NFFTs.* SIAM J. Sci. Comput., 24:2013–2037, 2003.

[42] D. Potts, G. Steidl, and M. Tasche: *Fast Fourier transforms for nonequispaced data: A tutorial.* In J.J. Benedetto and P.J.S.G. Ferreira (eds.): *Modern Sampling Theory: Mathematics and Applications*, pp. 247–270, Boston, MA, USA, 2001. Birkhäuser.

[43] G. Steidl: *A note on fast Fourier transforms for nonequispaced grids.* Adv. Comput. Math., 9:337–353, 1998.

[44] A.K. Tornberg and L. Greengard: *A fast multipole method for the three-dimensional Stokes equations.* Journal of Computational Physics, 227(3):1613 – 1619, 2008, ISSN 0021-9991.

[45] U. Trottenberg, C.W. Oosterlee, and A. Schuller: *Multigrid.* Academic Press, Inc., Orlando, FL, USA, 2000, ISBN 0-12-701070-X.

[46] Z.W. Wang and C. Holm: *Estimate of the cutoff errors in the Ewald summation for dipolar systems.* J. Chem. Phys., 115:6277–6798, 2001.

[47] A.F. Ware: *Fast approximate Fourier transforms for irregularly spaced data.* SIAM Rev., 40:838–856, 1998.